Department of Precision and Microsystems Engineering

2D Lattice Materials for Actuation

W.E.D. Nelissen

Report no : 2018.003
Coach : Dr. C. Ayas
Professor : Prof.dr.ir. A. van Keulen
Specialisation : Engineering Mechanics
Type of report : Master thesis
Date : 19-2-2018

TU Delft Delft University of Technology

Challenge the future

Summary

In the last two decades, lattice materials have received attention as a means to design adaptive structures. Being closely related to foams, lattice materials are similarly lightweight but, depending on their micro-architecture, can be much stiffer and stronger. Externally triggered lengthening or shortening (actuation) of one or more members in a lattice material can be used to achieve macroscopic shape changes.

The three main attributes sought in 2D lattice materials to be deemed suitable for actuation are in-plane isotropy, high specific elastic moduli and limited energy requirement for actuation. However, no infallible topological criteria have yet been discovered that determine which micro-architectures meet these requirements. The Kagome micro-architecture yields the best-performing lattice material for actuation known to date. It has the highest possible isotropic macroscopic elastic moduli, while bending-dominated deformation results when it is actuated, limiting the energy required.

This thesis contributes to the search for micro-architectures that perform similar to Kagome lattice material, or even outperform it. Four novel micro-architectures are introduced. Matrix analysis is performed on repetitive pin-jointed trusses with these designs. This analysis reveals the states of self-stress and linearised mechanisms of the structures. Macroscopic elastic properties of the rigid-jointed lattice materials are determined using finite element analysis with periodic boundary conditions. FE models comprising thousands of unit cells are employed to determine actuation energies associated with the different micro-architectures. These models also allow the effects of actuation to be quantified by the distance from an actuator at which the deformations vanish.

Each of the new micro-architectures is verified to constitute a stiff (i.e. stretching-dominated) isotropic lattice material. Still, not all of them result in optimal elastic moduli. One of the proposed designs does perform identically to the Kagome structure in terms of elastic moduli. Moreover, it requires less energy for actuation in the range of relative densities of interest. On the other hand, its attenuation distance is shorter; actuation deformations damp out within a shorter distance in comparison to Kagome lattice material.

Acknowledgements

I would like to thank my supervisor Dr. Can Ayas for being a source for motivation and insight throughout this project. I'm also grateful towards Dr. Cihan Tekoglu, his and Can's interest in lattice materials sparked my enthusiasm for the subject. The near-weekly meetings I had with Can as well as the conference calls we had with the three of us made for fruitful discussions and critical thinking. Helping me find direction when necessary while giving me freedom whenever possible resulted in a, in my opinion, successful research project.

W.E.D. Nelissen
Delft, February 2018

Contents

1 Introduction

This chapter gives a general introduction to this research project. Going over the most important advances in literature, the scope and aim of the project are sketched. Research objectives are set, after which an outline of the report concludes the chapter.

1.1. Lattice materials

Lattice materials are a type of cellular solids characterised by a clear repetitive structure. An example is shown in Fig. 1.1a. The high degree of order is in contrast to the stochastic nature of other cellular solids. Open cell foams for example, such as the one shown in Fig. 1.1b, comprise members having a range of dimensions that are randomly connected. Because of their highly structured nature, lattice materials can be stiffer and stronger than foams, at similar densities. As the mechanical behaviour of a foam is the combined result of cells with random layouts and many different sizes, the representative volume element that accurately mimics a foam's macroscopic properties is relatively large. The repetitive structure of a lattice material, on the other hand, can be described by a small periodic unit cell with a specific micro-architecture composed of a few lattice members. In case of a 2D lattice material, a planar unit cell of struts tessellates the plane while the unit cell (volume) of a 3D lattice material tessellates space. The slender lattice members act as bars or beams. Cellular solids could be synthesised from any base material. Metals are often the materials of choice for structural purposes e.g. Fig. 1.1a, but polymers and even ceramics are also applied, see for example the work of Zheng et al. [30].

The term *lattice material* is used emphasise that the lattice behaves as a *material*: it can be treated as a ho-

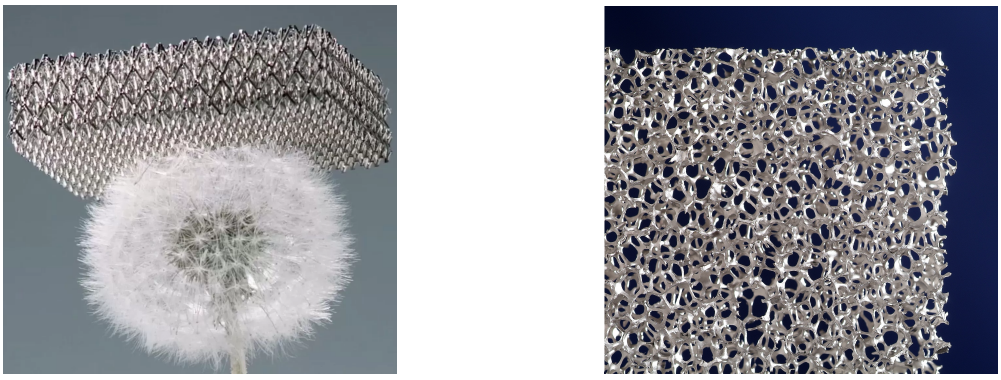

(a) (b)

Figure 1.1: Two examples of cellular solids. (a) A 3D lattice material developed by Boeing; made up out of hollow nickel-phosporus alloy tubes, 'Microlattice' consists of 99.99% air [25]. (b) An open-cell foam produced by Fraunhofer IFAM [16]. Note how the lattice material is highly structured, different from the more random geometry of the foam.

mogenised continuum with macroscopic properties such as elastic moduli and yield strength [21, 27]. This is justified when both the global length scale of the lattice and the wavelength(s) of loading are much larger than the dimensions of the unit cell. Lattices that do not comply with these requirements behave as a structure and hence are not classified as lattice materials. The macroscopic properties of a lattice material are dictated by three factors: material properties of the strut material, relative density $\bar{\rho}$ and micro-architecture [1]. The effect of the first two factors on a material property of interest are relatively straightforward. Ultimately, the lattice micro-architecture offers the key design freedom to control the macroscopic properties.

Relative density

Relative density $\bar{\rho}$ is a commonly employed parameter when comparing properties of cellular solids. It is defined [10] as the density of the cellular material ρ^* divided by ρ_s, the density of the solid material it is made of:

$$\bar{\rho} = \rho^* / \rho_s. \tag{1.1}$$

It can be determined simply as the volume fraction of the unit cell occupied by members. In the 2D case, considering members with identical rectangular cross-sections and neglecting sizing of joints, it is equal to the sum of the member lengths $l^{(i)}$ multiplied by the in-plane bar width w, divided by the unit cell area A_c:

$$\bar{\rho} = \frac{1}{A_\mathrm{c}} \sum_{i=1}^{N} l^{(i)} w, \tag{1.2}$$

where N is the number of members in the unit cell.

Actuation

In the last two decades, lattice materials have drawn attention in the context of shape morphing/adaptive materials. Shape morphing structures can be constructed by replacing some of the members of a lattice with actuators, where an *actuator* is a member with the ability to lengthen or shorten in response to an external stimulus. The change of length of these actuators causes deformations in the lattice [6, 14, 28]. Depending on the micro-architecture, deformation is either confined to a small area in the vicinity of the actuator or it spreads over a larger region. The latter type of structures are of interest, as actuation of such a lattice material can result in a macroscopic shape change.

Three-dimensional active lattice materials may seem the obvious choice for designing adaptive 3D devices, but planar lattice materials can also be used to construct 3D shape morphing structures. For example, a sandwich panel can be constructed featuring a planar active lattice material on one or both of its face sheets, and a core made of foam or regular 3D lattice material. Actuation of the planar lattice(s) causes the sandwich to deform. Depending on the lattice micro-architecture and placement of the actuators, both planar and out-of-plane deformation of the sandwich structure can be achieved [7, 8, 14, 29].

Stretching- and bending-dominated deformation

Two distinct types of deformation are encountered when lattice materials are subjected to external loads: deformation is dominated either by stretching or by bending of struts. The former results in higher macroscopic elastic moduli since the axial stiffness of slender struts is much higher than their bending stiffness.

Whether a lattice material is stretching- or bending-dominated can be determined from the static/kinematic properties of a pin-jointed truss with the same micro-architecture. If the repetitive truss does not have any inextensional mode of deformation (mechanism) that is associated with a macroscopic strain state, the corresponding rigid-jointed lattice material is stretching-dominated. Conversely, presence of one or more of such mechanisms for the repetitive pin-jointed truss implies bending-dominated deformation of the equivalent rigid-jointed lattice material. The macroscopic elastic moduli of a stretching-dominated lattice material scale linearly with relative density $\bar{\rho}$ whereas for a bending-dominated lattice material, macroscopic elastic moduli scale with $\bar{\rho}^2$ (3D) or $\bar{\rho}^3$ (2D lattice materials) [5, 9, 10, 27].

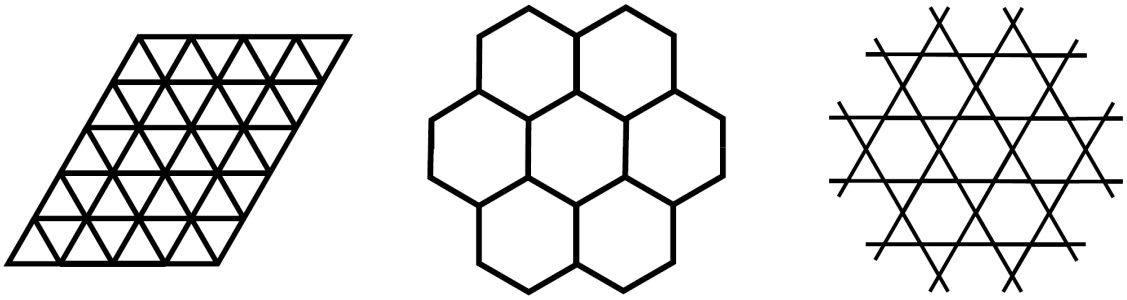

(a) (b) (c)

Figure 1.2: The three lattice material topologies studied in [28]: (a) Triangular, (b) Hexagonal and (c) Kagome micro-architecture. Figures from [23].

Actuation energy

The resistance of a lattice material to actuation is also micro-architecture-dependent and can be quantified by the amount of strain energy that is stored after actuating a single member in a large lattice. Single member actuation of three lattice materials with different layouts was first investigated by Wicks and Guest [28] by means of calculating actuation energy using finite element analysis. This study revealed that the triangulated lattice (Fig. 1.2a), with no mechanisms when pin-jointed, consumes significantly more energy than the bending-dominated hexagonal lattice (Fig. 1.2b). The pin-jointed hexagonal truss possesses mechanisms. The third investigated micro-architecture is the Kagome structure (Fig. 1.2c). Although the pin-jointed Kagome truss features a mechanism, rigid-jointed Kagome lattice material does exhibit high specific elastic properties due to stretching-dominated deformation behaviour. For a given value of $\bar{\rho}$, its effective elastic moduli are equal to those of the triangulated lattice [15, 27]. Conversely, energy consumed by Kagome lattice material under actuation is significantly less compared to triangulated lattice material. Still, more energy is required than in case of the hexagonal micro-architecture.

Applications

Many problems can be identified where 2D shape morphing materials may be applied. One example is that of an aeroplane wing, where changing for instance the wing's curvature) during flight has several benefits over conventional methods for manipulating aerodynamics, see Vigliotti and Pasini [26]. In any application where varying aero- or hydrodynamics are involved, designs with shape-morphing skins are of interest. For instance think of windmill and helicopter rotor blades, or high-end kayak paddles.

Mai and Fleck [19] investigated the use of 2D lattices as the skin of circular tubes. The study not only considered structural rigidity but also the possibility to change the macroscopic shape of a tube by actuation of the skin.

1.2. Motivation and objectives

The ideal lattice material for actuation [24] features high macroscopic elastic moduli and strength, such that it can be used for structural purposes. Isotropic elasticity is desirable in order for the lattice material to exhibit high stiffness irrespective of the loading direction. Finally, the lattice material should be compliant in response to actuation when selected members are replaced by actuators. Simultaneous fulfilment of these requirements is rare, as lattice layouts with high structural stiffness will generally show large resistance to actuation-driven deformation too. This does not rule out all lattice materials from being used in active structures, but requires a careful investigation of the elastic deformation characteristics of lattice materials with different micro-architectures.

The Kagome micro-architecture complies with all of the requirements above. Therewith it is currently unmatched in its performance as a planar actuation lattice material. The unique properties it yields triggered a search for other actuation-suited 2D lattice material designs. This thesis details a research project aimed at finding such micro-architectures and getting a better understanding of the mechanical behaviour of two-

dimensional lattice materials. Pronk et al. [24] recently proposed a set of (topological) criteria a 2D lattice material should satisfy to possess the hard to combine properties of an ideal actuation material. With these novel criteria in mind, the following objectives are defined

- Find 2D repetitive micro-architectures that result in properties that are similar to those of Kagome lattice material: isotropic and stiff, with limited resistance to actuation.
- In doing so, apply and test the criteria for a lattice material to be suitable for actuation proposed by Pronk et al. [24].
- Compare lattice materials with different micro-architectures. Not only regarding macroscopic mechanical properties and actuation energy, but also by the effects of actuation.

1.3. Outline

Following the general introduction given in this chapter, the static and kinematics properties of finite and infinite structures are discussed in Chapter 2. First, a short review of matrix analysis for pin-jointed structures is given. Then, the concepts of statical and kinematical determinacy are illustrated for finite structures, after which definitions of determinacy are given for repetitive (infinite) structures. The chapter concludes with a description of the proposed criteria for actuation-suited lattice materials of Pronk et al [24].

In Chapter 3, a number of candidate micro-architectures are introduced and it is explained how they were contrived. Geometrical similarities and differences are discussed, based on which expectations are formed regarding the mechanical performance of lattice materials with the proposed micro-architectures.

Using the matrix method, static and kinematic properties of pin-jointed repetitive trusses with the candidate designs are determined in Chapter 4. Mechanisms and states of self-stress are identified, allowing for conclusions to be drawn regarding statical and kinematical determinacy of the structures.

Chapter 5 details how the macroscopic elastic properties of the rigidly jointed lattice materials are determined using the finite element (FE) method. Numerically efficient FE models are considered that make use of symmetry and periodic boundary conditions. Young's and Shear moduli are presented as a function of relative density, as well as Poisson's ratios.

Large FE models representing large sheets of the lattice materials under investigation are presented in Chapter 6. The results from these models allow the actuation performance of the different micro-architectures to be determined. Actuation energies are calculated according to the methods found in literature. In addition, the effects of actuation are quantified by a measure of how far deformations spread away from an actuator.

In Chapter 7, the most important results of the different analyses are summarised and discussed. Some of the novel micro-architectures have surprising combinations of properties, which would not have been predicted based on insights from recent literature. One proposed lattice material design compares exceptionally well against Kagome, both in mechanical terms and regarding actuation.

The most important conclusions drawn from the research are briefly summarised in Chapter 8.

Chapter 9 presents an outlook and recommendations for future research directions.

Supplementary information is listed in the appendices: Appendices A and B contain additional data regarding the matrix analyses described in Chapter 4; large matrices that do not fit the main text conveniently. Appendix C briefly summarises the general derivation of boundary conditions such as those applied in Chapter 5. Appendix D contains another addition to Chapter 5; the deformations and forces occurring in two closely related lattice materials are compared. Appendix E summarises matrix analysis of a triangulated repetitive pin-jointed truss, the results of which are part of the discussion in Chapter 7.

2

Statics and kinematics of infinite structures

The mechanical properties of a lattice material with a certain micro-architecture of rigidly connected struts are closely related to the static/kinematic properties of its pin-jointed counterpart. Therefore, the concepts of statical and kinematical determinacy, which are central in determining the rigidity of a pin-jointed truss, are also key to identifying stretching-dominated lattice materials with high stiffness. Statics and kinematics of finite and infinite pin-jointed trusses are shortly revisited here. Then it is discussed how the latter translate into mechanical properties of lattice materials.

2.1. Equilibrium and compatibility equations

Consider an n-dimesional pin-jointed truss comprising b bars that connect j joints. The structure is fixed to its surroundings by k foundational constraints. Equilibrium equations can be set up, relating the external forces acting on joints to the tensions arising in the bars of the structure. In matrix form, the $(nj-k)\times b$ equilibrium matrix $\boldsymbol{A}$, post-multiplied with the $b\times 1$ vector of bar tensions $\boldsymbol{t}$ yields the $(nj-k)\times 1$ nodal force vector $\boldsymbol{f}$, i.e.

$$\boldsymbol{A}\boldsymbol{t}=\boldsymbol{f}. \tag{2.1}$$

The nullspace (kernel) of $\boldsymbol{A}$ represents all combinations of bar tensions that are in equilibrium with zero nodal loads; i.e. non-zero solutions of $\boldsymbol{t}$ that satisfy $\boldsymbol{A}\boldsymbol{t}=\boldsymbol{0}$. Such solutions are called states of self-stress and exist if $\boldsymbol{A}$ is not of full rank.

A kinematic assessment of the truss yields another system of equations that can be cast into matrix form:

$$\boldsymbol{B}\boldsymbol{d}=\boldsymbol{e}, \tag{2.2}$$

where $\boldsymbol{d}$ is the $(nj-k)\times 1$ nodal displacement vector and $\boldsymbol{e}$ is the $b\times 1$ vector of bar elongations. $\boldsymbol{B}$ is the $b\times(nj-k)$ compatibility matrix. Static and kinematic analyses of a pin-jointed truss are equivalent; $\boldsymbol{B}=\boldsymbol{A}^{\mathrm{T}}$ by virtue of the principle of virtual work. The nullspace of $\boldsymbol{B}$ contains inextensional displacement modes: non-zero displacement vectors $\boldsymbol{d}$ that satisfy Eq. (2.2) for $\boldsymbol{e}=0$. Such a displacement mode is either a rigid-body translation or rotation, or it represents a mechanism.

Mechanisms

Mechanisms can be classified into infinitesimal and finite mechanisms. For finite mechanisms, joints can displace by finite amounts while the length of each member of the truss is preserved. An infinitesimal mechanism on the other hand leads to small changes in one or more members' lengths. The meaning of 'small' here being that the elongation (positive or negative) is of second or higher order in terms of joint displacements. Consequently, infinitesimal mechanisms tighten up after infinitesimally small displacements of joints.

A key assumption in matrix analysis is that the displacements of joints are so small that the equilibrium and compatibility equations for the original (undeformed) configuration remain accurate, i.e. the static and kinematic equations are linearised in the undeformed configuration. The linearised mechanisms found through

matrix analysis therefore represent mechanisms that in reality can be either infinitesimal or finite. The analysis cannot distinguish between the two. Determining the actual nature of a mechanism can be done by subjecting a structure to that mechanism, taking into account non-linear kinematic effects. If the lengths of all bars in the truss remain unchanged, the mechanism is finite. Otherwise the mechanism is infinitesimal.

2.2. Finite structures

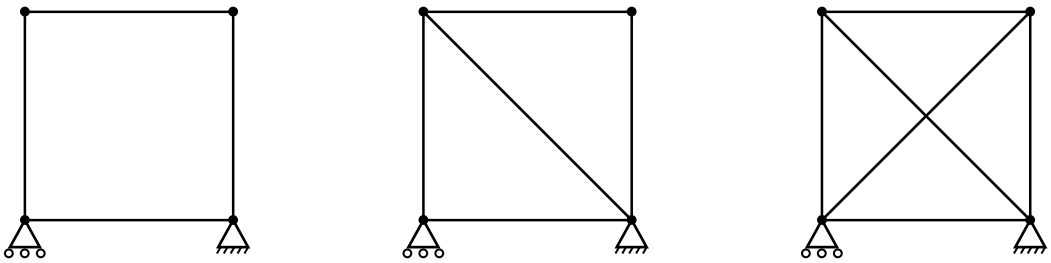

(a) (b) (c)

Figure 2.1: Textbook examples of finite pin-jointed trusses: (a) is kinematically indeterminate, (b) is both statically and kinematically determinate and (c) is statically indeterminate. Note that the 2 rigid-body translations and rigid-body rotations are suppressed by three foundational constraints.

Fig. 2.1 illustrates three finite pin-jointed trusses. Each of them is supported by three foundational constraints. The bottom-right corner is fixed in both the horizontal and the vertical direction. The bottom-left corner has a roller support, which only blocks vertical displacement.

The structure in Fig. 2.1a clearly has a mechanism; if a horizontal displacement is imposed on either of its two top nodes, it will offer no resistance and collapse. A structure that is capable of one or more such mechanisms is kinematically indeterminate.

The truss depicted in Fig. 2.1b on the other hand is rigid; no matter the applied load(s), the structure will resist and keep its shape. If however one of the struts were to be lengthened or shortened, the structure would change shape. The resulting nodal positions are unique, i.e. if the elongation of each member is known, the resulting positions of the nodes can be calculated; the structure is kinematically determinate. Also, it is impossible for any of the bars of the structure in Fig. 2.1b to sustain a tensile or compressive force, in the absence of external forces on the nodes; equilibrium would not be satisfied in the nodes. In other words, the truss is not capable of states of self-stress, and is called statically determinate.

The structure in Fig. 2.1c is also rigid. The second diagonal member however is not required for rigidity. This redundant strut makes that the truss is statically indeterminate. It is capable of one state of self-stress; a combination of bar forces that is in equilibrium with zero nodal loads.

A finite truss with k foundational constraints can be both statically and kinematically determinate if it satisfies Maxwell's stability criterion [20],

$$b - nj + k = 0, \tag{2.3}$$

where $n = 2$ for a two-dimensional truss and $n = 3$ in case of a three dimensional truss, and j is the total number of joints. To constrain all rigid-body displacements, for a planar truss $k = 3$, while in 3D $k = 6$. Eq. (2.3) is satisfied if the number of bars b is equal to the number of unconstrained nodal displacements $nj - k$. However, rigidity is acquired only if the bars are properly positioned.

Remember that the equilibrium matrix $\boldsymbol{A}$ of a finite truss has dimensions $(nj - k) \times b$, and its compatibility matrix $\boldsymbol{B}$ is of size $b \times (nj - k)$. Thus, if the structure satisfies Eq. (2.3), it has square matrices $\boldsymbol{A}$ and $\boldsymbol{B}$ as $nj - k = b$.

The three trusses in Fig. 2.1, were used to illustrate the meaning of statical and kinematical determinacy. A statically determinate structure is incapable of sustaining self-stress, while a kinematically determinate truss has no mechanisms. States of self-stress are represented by the vectors in the nullspace of $\boldsymbol{A}$ and mechanisms appear in null($\boldsymbol{B}$). A simultaneously statically and kinematically determinate structure such as the one in

Fig.2.1b thus has $\boldsymbol{A}$- and $\boldsymbol{B}$-matrices that both are of full rank. It was mentioned earlier that $\boldsymbol{A}^{\mathrm{T}} = \boldsymbol{B}$; the implication of that is that the rank of $\boldsymbol{B}$ is always equal to the rank of $\boldsymbol{A}$. Therefore, these matrices must be square to possibly be of full rank simultaneously. These matrices being square is exactly what Maxwell's stability criterion enforces. Still, the rule does not guarantee them to be of full rank. That is, the Maxwell condition $b = nj - k$ is a necessary but not sufficient criterion for statical and kinematical determinacy of a finite truss.

2.3. Infinite structures

Since a lattice material by definition consists of a very large number of unit cells, it is appropriate to investigate the rigidity of the equivalent repetitive pin-jointed truss for an indication of its mechanical performance, see Deshpande et al. [5]. A repetitive structure is infinitely large but can be represented by a (single) periodic unit cell: loads and deformations are assumed to repeat with the repetition of that unit cell through n-dimensional space. The unit cell geometry represents the micro-architecture of the corresponding lattice material.

While it is intuitively clear what a rigid a finite truss is, it is not so straight-forward what rigidity of an infinite repetitive truss means. Guest and Hutchinson [11] suggested that for a 2D repetitive truss to be rigid from a statics point of view, it must be able to sustain any combination of the three possible macroscopic (remote) stresses in the plane, σ_{11}, σ_{22} and σ_{12}, with zero nodal forces ($\boldsymbol{f} = \boldsymbol{0}$). This implies that $\boldsymbol{A}$ is rank-deficient by *at least* three: the truss has three or more states of self-stress, which are represented by the vectors in the nullspace of $\boldsymbol{A}$. Using the method of sections, (linear combinations of) these states of self-stress must evaluate to the three possible macroscopic stresses.

There is also no generally accepted definition of static and kinematic determinacy for a infinite repetitive truss. With the requirement for rigidity described above, static determinacy can be defined: a 2D repetitive structure is statically determinate if there are *exactly* three non-zero solutions to the equilibrium equations $\boldsymbol{At} = \boldsymbol{0}$, that correspond to the three possible remote loadings in 2D.

A unit-cell periodic model of an infinite truss comes with limitations. First, rigid-body rotations are impossible. As nodal displacements are periodic, they are identical for every instance of the unit cell. During rigid-body rotation, displacements at a given point are dependent on the distance from that point to the centre of rotation. Thus, only rigid-body translation modes remain. Secondly, it is impossible to apply foundational constraints to suppress the remaining rigid body-displacements, as is done for the finite structures in Fig. 2.1. Namely, a single foundational constraint on any of the nodes of the unit cell directly results in infinitely many constraints throughout the repetitive truss.

It was just explained that foundational supports cannot be applied, and that only rigid-body translations, not rotations, are possible in a periodic model. Therefore, a kinematically determinate 2D repetitive truss can be defined as one where the only solutions to the compatibility equations for $\boldsymbol{e} = \boldsymbol{0}$ are the two rigid body translations, ruling out the existence of mechanisms, see Guest and Hutchinson [11]. Therewith, this study concluded that if a repetitive pin-jointed truss is kinematically determinate, it cannot be statically determinate, and vice versa.

Criteria for actuation-suited micro-architectures

Pronk et al. pointed out in [24] that the simultaneous requirement of high stiffness and low-energy actuation is the main challenge in the search for the ideal lattice micro-architecture for actuation. That is, the rigid-jointed lattice material must deform in a stretching-dominated manner in response to macroscopic loads, while when one or more bars are replaced with actuators, a length change of an actuator should cause the surrounding lattice to deform compliantly; actuation must cause bending-dominated deformation.

After thorough analysis of a number of lattice micro-architectures, Pronk et al. [24] proposed that for an isotropic 2D lattice material to be suitable for actuation, its pin-jointed counterpart must be statically determinate and satisfy Maxwell's stability criterion. The latter was generalised by Pellegrino and Calladine [22] to

$$s - m = b - nj + k = 0, \tag{2.4}$$

where s is the number of states of self-stress and m is the number of inextensional displacement modes. As the number of foundational constraints $k = 0$ for a periodic truss and $s = 3$ if it is statically determinate, such a structure must have one mechanism. Pronk et al. [24] conjectured that the appearing mechanism must be *non strain-producing*.

The key characteristic of a non strain-producing mechanism is that its linearised version does not induce any macroscopic strain. Vice versa, such a mechanism is not excited when the repetitive structure endures macroscopic strain. Thus, a non strain-producing mechanism of its pin-jointed equivalent does not allow a lattice material to be strained macroscopically without members being stretched or compressed. In contrast, actuation of a member may exploit the mechanism-like character of the architecture, causing the lattice material to deform in a bending-dominated fashion. The latter results in low energy requirement for actuation.

In summary, for a lattice material to be suitable for actuation, Pronk et al. [24] proposed that its pin-jointed equivalent must satisfy the following criteria:

- It satisfies Maxwell's stability criterion (Eq. (2.4)) with no foundational constraints, i.e. for $k = 0$.
- It is statically determinate according to the definition of Guest and Hutchinson [11].
- The mechanism it consequently possesses must be non strain-producing.

3

Introduction of four novel micro-architectures

Remember that a 2D lattice material suitable for actuation must be in-plane isotropic and feature high macroscopic elastic moduli, while requiring a limited amount of energy for actuation. To date, no micro-architectures for 2D actuation lattice materials have been proposed in literature that can compete with the Kagome structure. The four regular tilings of the plane were readily exhausted, while all the semi-regular tessellations other than Kagome were recently proved unsuitable by Pronk et al. [24]. Still, since there are infinitely many ways to tessellate the plane, even merely with regular polygons [2], it is very unlikely that actuation suitability is indeed unique to the Kagome micro-architecture.

A series of new lattice material micro-architectures is shown in Fig. 3.1. The first three micro-architectures, displayed in Fig. 3.1a-c are all closely related to the Kagome lattice. The **K**agome with concentric **T**riangles (KT) structure is attained by dissecting each triangle in a Kagome lattice into four equilateral triangles of equal size; see Fig. 3.1a. Similarly, **K**agome with concentric **H**exagons (KH) features an additional concentric hexagon within each hexagon that is present in a regular Kagome lattice; see Figure 3.1b. The **D**ouble **K**agome (DK) structure is shown in Fig. 3.1c. For each (infinitely long) set of aligned members appearing in the Kagome structure, the DK structure features two parallel lines.

The fourth micro-architecture considered is the **M**odified **D**odecagonal structure (MD), depicted in Fig. 3.1d. It is based on the 2-uniform '3-4-6-12 tiling' [4]. Dodecagons are the largest polygons appearing in the 3-4-6-12 tiling. The MD structure is constructed by dissecting all of the hexagons in the 2-uniform tiling into two equilateral triangles and two rhombi. This is done such that the axes of six- and three-fold symmetry are preserved; all structures shown in Fig. 3.1 are in-plane isotropic owing to axes of three-fold rotational symmetry [3]. The MD structure is closely related to the Hexagonal Cupola architecture. The latter was investigated by Pronk et al. in [24]. The study concluded it is not suitable for actuation purposes because of its bending-dominated deformation behaviour. The structure presented in Figure 3.1d is expected to have more favourable mechanical properties. The reason for this is the fact that there are no uninterrupted (infinite)

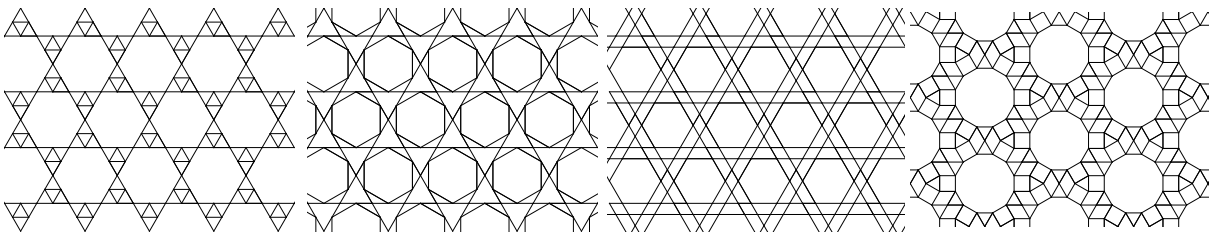

(a) (b) (c) (d)

Figure 3.1: Lattice micro-architectures investigated: (a) Kagome with concentric triangles (KT), (b) Kagome with concentric hexagons (KH), (c) Double Kagome (DK) and (d) the 'modified dodecagonal structure' (MD).

arrays of parallel members in the MD structure, which there are in each of the Hexagonal, Hexagonal Cupola and 3-4-6-12 architectures. All of the latter are bending-dominated.

It is readily apparent that the three Kagome-related micro-architectures contain continuous sets of aligned members. Clearly, if a lattice material with any of these designs were to sustain a macroscopic tensile stress aligned with one of these sets, part of the struts would surely be loaded purely axially. This should translate into stretching-dominated properties in at least these directions. But, as just mentioned, all proposed structures feature planar isotropy due to their symmetry; high, direction-independent elastic moduli are anticipated. In the MD structure on the other hand, no uninterrupted sets of aligned members appear. It remains to be seen how the effective elastic moduli of lattice materials with these micro-architectures compare.

All presented micro-architectures have a valency of four, i.e. all joints connect 4 members. Therefore $b = 2j$ in Eq. (2.4) [5]. Therewith the structures fulfil the first of the proposed criteria for actuation-suitability and thus have square equilibrium and compatibility matrices. The micro-architectures depicted in Figs. 3.1a and d have a uniform member length whereas KH and DK feature members of two different lengths.

4

Matrix analysis of novel micro-architectures

This section describes matrix analysis of the novel structures presented in Chapter 3. Section 4.1 covers the kinematics, statics are discussed in section 4.2. Detailed descriptions of the analyses of the KT architecture are given, followed by a summary of and comparison with results for the other structures.

4.1. Inextensional displacement modes

Conventional matrix analysis of a repetitive truss concerns only displacements of nodes within the chosen unit cell. The unit cells selected for matrix analysis of the introduced micro-architectures are shown in Fig. 4.1. Nodes are labelled with regular digits, strut numbers are indicated by Roman numerals. Note that the unit cells are selected such that no nodes are located on unit cell boundaries. If there are nodes on the boundary of a unit cell, duplicate nodes appear that complicate the analysis.

Consider the KT unit cell in Fig. 4.1a. It contains nine internal nodes with a total of 18 independent nodal displacements: $\boldsymbol{d} = [d_1^{(1)}\ d_2^{(1)}\ \ldots\ d_1^{(9)}\ d_2^{(9)}]^{\mathrm{T}}$, where $d_i^{(J)}$ denotes the displacement in the x_i-direction of node J. Coordinate systems are indicated in Fig. 4.1. Remember Eq. (2.2); the vector of member elongations $\boldsymbol{e} = [e^{\mathrm{I}}\ \ldots\ e^{\mathrm{XVIII}}]^{\mathrm{T}}$ is directly related to the nodal displacement vector through the 18×18 compatibility matrix $\boldsymbol{B}$,

$$\boldsymbol{B}\boldsymbol{d} = \boldsymbol{e}. \tag{2.2}$$

The entries of the compatibility matrix are determined from the unit cell geometry. Some members cross a cell boundary. Still, periodicity in both the x_1- and x_2-direction causes these members to effectively be connected to two nodes within the same cell. For instance, member XV in Fig. 4.1a connects nodes 1 and 8.

Deformation of the unit cell is not considered in conventional matrix analysis of periodic structures. Therefore, no information is gathered on inextensional displacement modes that affect the size and shape of the unit cell. Mechanisms that distort the unit cell are determined using the augmented matrix method. To quantify straining of the unit cell, three unit cell deformations are defined:

$$\begin{aligned} d_{11} &= 2l_0\varepsilon_{11}, \\ d_{22} &= l_0\sqrt{3}\varepsilon_{22}, \\ d_{12} &= 2l_0\varepsilon_{12}, \end{aligned} \tag{4.1}$$

which are the three planar strains ε_{ij} multiplied by characteristic lengths of the unit cell. Any length scale may be used, but width and/or height of the unit cell are a convenient choice. The unit cell deformations are appended to $\mathbf{d}$ to construct the 21×1 augmented displacement vector:

$$\boldsymbol{d}_{\mathrm{aug}} = [d_1^{(1)}\ d_2^{(1)}\ d_1^{(2)}\ d_2^{(2)}\ \ldots\ d_1^{(8)}\ d_2^{(8)}\ d_1^{(9)}\ d_2^{(9)}\ d_{11}\ d_{12}\ d_{22}]^{\mathrm{T}}. \tag{4.2}$$

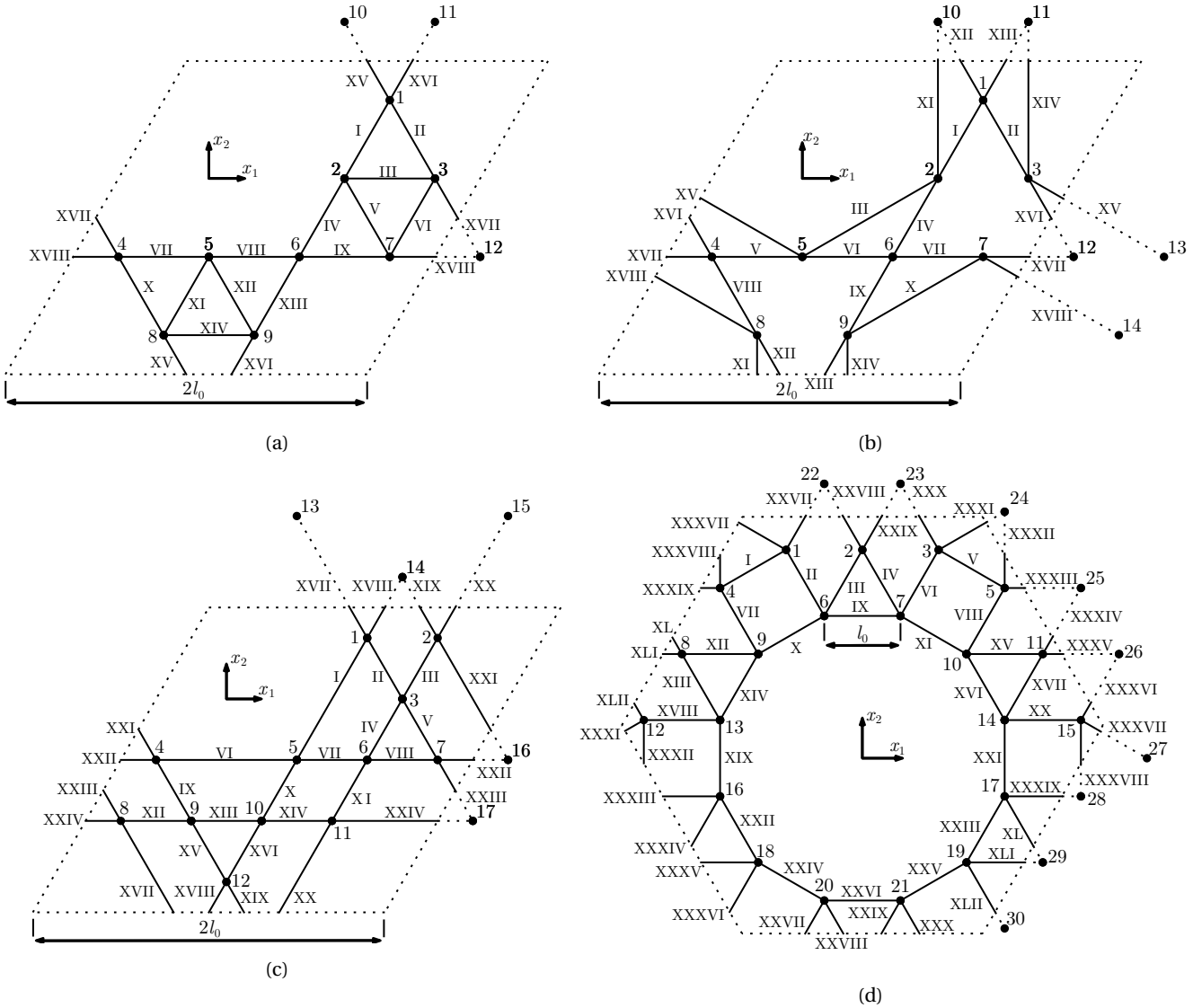

Figure 4.1: Selected unit cells for matrix analysis of the pin-jointed versions of the new micro-architectures. Node and bar numbers are indicated. Nodes are labelled with regular digits. Struts are labelled with Roman digits.

The augmented nodes (numbers 10, 11 and 12 in case of KT) represent nodes in adjacent cells. Their displacements can be expressed in terms of displacements of internal nodes and the unit cell deformations:

$$\begin{aligned} d_1^{(10)} &= d_1^{(8)} + \frac{1}{2}d_{11} + \frac{\sqrt{3}}{2}d_{12}, & d_2^{(10)} &= d_2^{(8)} + \frac{1}{2}d_{12} + d_{22}, \\ d_1^{(11)} &= d_1^{(9)} + \frac{1}{2}d_{11} + \frac{1}{2}d_{12}, & d_2^{(11)} &= d_2^{(9)} + \frac{1}{2}d_{12} + d_{22}, \\ d_1^{(12)} &= d_1^{(4)} + d_{11}, & d_2^{(12)} &= d_2^{(4)} + d_{12}. \end{aligned} \tag{4.3}$$

In regular matrix analysis, members crossing a boundary, such as member XV, effectively connected two internal nodes of the same unit cell. Using the augmented nodal displacements defined in Eq.(4.3), the elongations of these members can now be expressed in terms of displacements of nodes in adjacent cells. The kinematics of the structure become, similar to Eq. (2.2):

$$\boldsymbol{B}_{\text{aug}}\boldsymbol{d}_{\text{aug}} = \boldsymbol{e}. \tag{4.4}$$

The augmented compatibility matrix $\boldsymbol{B}_{\text{aug}}$ is constructed from $\boldsymbol{B}$ by taking into account the contributions of the unit cell deformations to the member elongations. These contributions can be represented by the 18×3 matrix $\boldsymbol{C}$. Appending $\boldsymbol{C}$ to the right side of $\boldsymbol{B}$ yields the augmented compatibility matrix:

$$\boldsymbol{B}_{\text{aug}} = [\boldsymbol{B}|\boldsymbol{C}] =$$

$$\left[\begin{array}{cccccccccccccccccc|ccc}
\frac{1}{2} & \frac{\sqrt{3}}{2} & -\frac{1}{2} & -\frac{\sqrt{3}}{2} & 0 & 0 & 0 & 0 & 0 & 0 & 0 & 0 & 0 & 0 & 0 & 0 & 0 & 0 & 0 & 0 & 0 \\
-\frac{1}{2} & \frac{\sqrt{3}}{2} & 0 & 0 & \frac{1}{2} & -\frac{\sqrt{3}}{2} & 0 & 0 & 0 & 0 & 0 & 0 & 0 & 0 & 0 & 0 & 0 & 0 & 0 & 0 & 0 \\
0 & 0 & -1 & 0 & 1 & 0 & 0 & 0 & 0 & 0 & 0 & 0 & 0 & 0 & 0 & 0 & 0 & 0 & 0 & 0 & 0 \\
0 & 0 & \frac{1}{2} & \frac{\sqrt{3}}{2} & 0 & 0 & 0 & 0 & 0 & 0 & -\frac{1}{2} & -\frac{\sqrt{3}}{2} & 0 & 0 & 0 & 0 & 0 & 0 & 0 & 0 & 0 \\
0 & 0 & -\frac{1}{2} & \frac{\sqrt{3}}{2} & 0 & 0 & 0 & 0 & 0 & 0 & 0 & 0 & \frac{1}{2} & -\frac{\sqrt{3}}{2} & 0 & 0 & 0 & 0 & 0 & 0 & 0 \\
0 & 0 & 0 & 0 & \frac{1}{2} & \frac{\sqrt{3}}{2} & 0 & 0 & 0 & 0 & 0 & 0 & -\frac{1}{2} & -\frac{\sqrt{3}}{2} & 0 & 0 & 0 & 0 & 0 & 0 & 0 \\
0 & 0 & 0 & 0 & 0 & 0 & -1 & 0 & 1 & 0 & 0 & 0 & 0 & 0 & 0 & 0 & 0 & 0 & 0 & 0 & 0 \\
0 & 0 & 0 & 0 & 0 & 0 & 0 & 0 & -1 & 0 & 1 & 0 & 0 & 0 & 0 & 0 & 0 & 0 & 0 & 0 & 0 \\
0 & 0 & 0 & 0 & 0 & 0 & 0 & 0 & 0 & 0 & -1 & 0 & 1 & 0 & 0 & 0 & 0 & 0 & 0 & 0 & 0 \\
0 & 0 & 0 & 0 & 0 & 0 & -\frac{1}{2} & \frac{\sqrt{3}}{2} & 0 & 0 & 0 & 0 & 0 & 0 & \frac{1}{2} & -\frac{\sqrt{3}}{2} & 0 & 0 & 0 & 0 & 0 \\
0 & 0 & 0 & 0 & 0 & 0 & 0 & 0 & \frac{1}{2} & \frac{\sqrt{3}}{2} & 0 & 0 & 0 & 0 & -\frac{1}{2} & -\frac{\sqrt{3}}{2} & 0 & 0 & 0 & 0 & 0 \\
0 & 0 & 0 & 0 & 0 & 0 & 0 & 0 & -\frac{1}{2} & \frac{\sqrt{3}}{2} & 0 & 0 & 0 & 0 & 0 & 0 & \frac{1}{2} & -\frac{\sqrt{3}}{2} & 0 & 0 & 0 \\
0 & 0 & 0 & 0 & 0 & 0 & 0 & 0 & 0 & 0 & \frac{1}{2} & \frac{\sqrt{3}}{2} & 0 & 0 & 0 & 0 & -\frac{1}{2} & -\frac{\sqrt{3}}{2} & 0 & 0 & 0 \\
0 & 0 & 0 & 0 & 0 & 0 & 0 & 0 & 0 & 0 & 0 & 0 & 0 & 0 & -1 & 0 & 1 & 0 & 0 & 0 & 0 \\
\frac{1}{2} & -\frac{\sqrt{3}}{2} & 0 & 0 & 0 & 0 & 0 & 0 & 0 & 0 & 0 & 0 & 0 & 0 & -\frac{1}{2} & \frac{\sqrt{3}}{2} & 0 & 0 & -\frac{1}{4} & 0 & \frac{\sqrt{3}}{2} \\
-\frac{1}{2} & -\frac{\sqrt{3}}{2} & 0 & 0 & 0 & 0 & 0 & 0 & 0 & 0 & 0 & 0 & 0 & 0 & 0 & 0 & \frac{1}{2} & \frac{\sqrt{3}}{2} & \frac{1}{4} & \frac{1+\sqrt{3}}{4} & \frac{\sqrt{3}}{2} \\
0 & 0 & 0 & 0 & -\frac{1}{2} & \frac{\sqrt{3}}{2} & \frac{1}{2} & -\frac{\sqrt{3}}{2} & 0 & 0 & 0 & 0 & 0 & 0 & 0 & 0 & 0 & 0 & \frac{1}{2} & -\frac{\sqrt{3}}{2} & 0 \\
0 & 0 & 0 & 0 & 0 & 0 & 1 & 0 & 0 & 0 & 0 & 0 & -1 & 0 & 0 & 0 & 0 & 0 & 1 & 0 & 0
\end{array}\right] \tag{4.5}$$

The rank of this 18×21 augmented compatibility matrix is 18, indicating it has a nullspace containing 3 linearly independent displacement modes:

$$\text{null}(\boldsymbol{B}_{\text{aug}}) = \left[\begin{array}{ccccccccccccccccccccc}
0 & 1 & 0 & 1 & 0 & 1 & 0 & 1 & 0 & 1 & 0 & 1 & 0 & 1 & 0 & 1 & 0 & 1 & 0 & 0 & 0 \\
1 & 0 & 1 & 0 & 1 & 0 & 1 & 0 & 1 & 0 & 1 & 0 & 1 & 0 & 1 & 0 & 1 & 0 & 0 & 0 & 0 \\
\sqrt{3} & -1 & \frac{\sqrt{3}}{2} & -\frac{1}{2} & \frac{\sqrt{3}}{2} & -\frac{3}{2} & 0 & -2 & 0 & -1 & 0 & 0 & 0 & -1 & \frac{\sqrt{3}}{2} & -\frac{3}{2} & \frac{\sqrt{3}}{2} & -\frac{1}{2} & 0 & 0 & 0
\end{array}\right]^{\text{T}}. \tag{4.6}$$

Note that the last three rows of null($\boldsymbol{B}_{\text{aug}}$) contain only zeroes: there is no strain associated with any of these linearised displacement modes. In fact, except for the added three zero entries, the vectors listed in Eq. (4.6) are equal to those that are in null($\boldsymbol{B}$).

The first and second columns of null($\boldsymbol{B}_{\text{aug}}$) represent rigid body translation in the x_2- and x_1-direction, respectively. The third column represents an infinitesimal increment of a unit cell-periodic finite mechanism, which is depicted in Fig. 4.2a. It is characterized by opposed rotations by equal amounts around node 6,

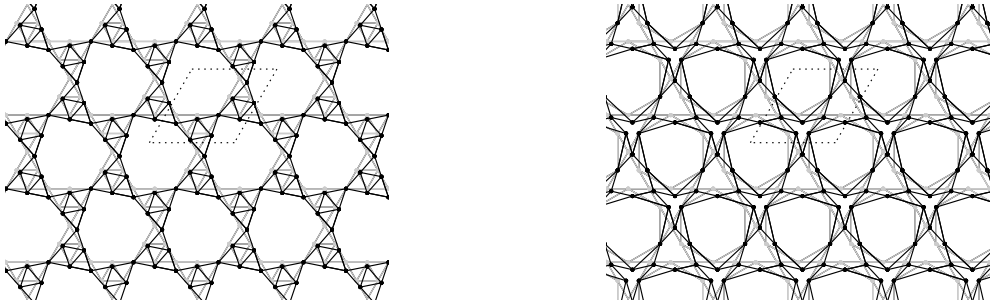

(a) (b)

Figure 4.2: Linearised representations of the unit cell periodic finite mechanisms of the (a) KT and (b) KH micro-architecture. The dotted lines form the outline of a unit cell for both the deformed (shown in black) and undeformed (shown in grey) configuration: there is no (macroscopic) strain associated with this increment of either of the finite mechanisms.

where two triangles meet. The Kagome micro-architecture possesses an equivalent unit cell-periodic mechanism [11]. Its linearised version is non strain-producing.

The KH structure features the exact same positioning of nodes as the KT structure, compare Figs. 4.1a and 4.1b. Only the connecting members are different. This micro-architecture therefore too yields a 18×21 augmented compatibility matrix; it is listed in Appendix A. Like the KT structure, the pin-jointed KH structure is capable of two rigid body displacements and one unit cell-periodic mechanism. The latter is depicted in Fig. 4.2b. The KH mechanism clearly differs from the mechanism the KT structure possesses. Still, the linearised version of the KH mechanism is non strain-producing too. The nullspace of $\boldsymbol{B}_{\text{aug}}$ for this structure is found in Appendix B.

Matrix analysis of the pin-jointed DK truss is performed using unit cell depicted in Fig. 4.1c. This unit cell contains 12 nodes, constituting a total of 24 independent displacements, and 24 members allowing for 24 member elongations. This results in a 24×27 augmented compatibility matrix (see Appendix A), the nullspace of which, listed in Appendix B, reveals there are *four* non strain-producing periodic mechanisms for this structure, in addition to two rigid-body translations. The linearised unit-cell periodic mechanisms are illustrated in Fig. 4.3.

Finally, the unit cell of the pin-jointed MD truss is depicted in Fig. 4.1d. It contains 21 nodes and 42 members. The resulting 42×45 augmented compatibility matrix $\boldsymbol{B}_{\text{aug}}$ is of rank 41; its nullspace contains four displacement modes that do not cause any member elongation. $\boldsymbol{B}_{\text{aug}}$ and null($\boldsymbol{B}_{\text{aug}}$) for the MD structure are listed in Appendix A and B, respectively. As for all other novel structures, two of the inextensional displacement modes are rigid-body translations. The two remaining periodic mechanisms are shown in Fig. 4.4. Both linearised mechanisms are non strain-producing.

All of the investigated micro-architectures have one or more periodic mechanisms. Augmented matrix analysis showed that each of these mechanisms is non strain-producing in the linear regime. Therefore, none of the mechanisms can be triggered by any 2D macroscopic load.

4.2. States of self-stress

Recall that a periodic pin-jointed truss with the KT micro-architecture has a square compatibility matrix $\boldsymbol{B}$. Therefore, its equilibrium matrix $\boldsymbol{A} = \boldsymbol{B}^{\text{T}}$ is also square. Recall Eq. (2.1),

$$\boldsymbol{A}\boldsymbol{t} = \boldsymbol{f}; \tag{2.1}$$

$\boldsymbol{A}$ relates the vector of bar tensions $\boldsymbol{t} = [t^{\text{I}} \ldots t^{\text{XVIII}}]^{\text{T}}$ to the vector of nodal forces $\boldsymbol{f} = [f_1^{(1)}\ f_2^{(1)} \ldots f_1^{(9)}\ f_2^{(9)}]^{\text{T}}$.

The nullspace of $\boldsymbol{A}$

$$\text{null}(\boldsymbol{A}) = \begin{bmatrix} 1 & 0 & 0 & 1 & 0 & 0 & 0 & 0 & 0 & 0 & 0 & 0 & 1 & 0 & 0 & 1 & 0 & 0 \\ 0 & 1 & 0 & 0 & 0 & 0 & 0 & 0 & 0 & 1 & 0 & 0 & 0 & 0 & 1 & 0 & 1 & 0 \\ 0 & 0 & 0 & 0 & 0 & 0 & 1 & 1 & 1 & 0 & 0 & 0 & 0 & 0 & 0 & 0 & 0 & 1 \end{bmatrix}^{\text{T}}, \tag{4.7}$$

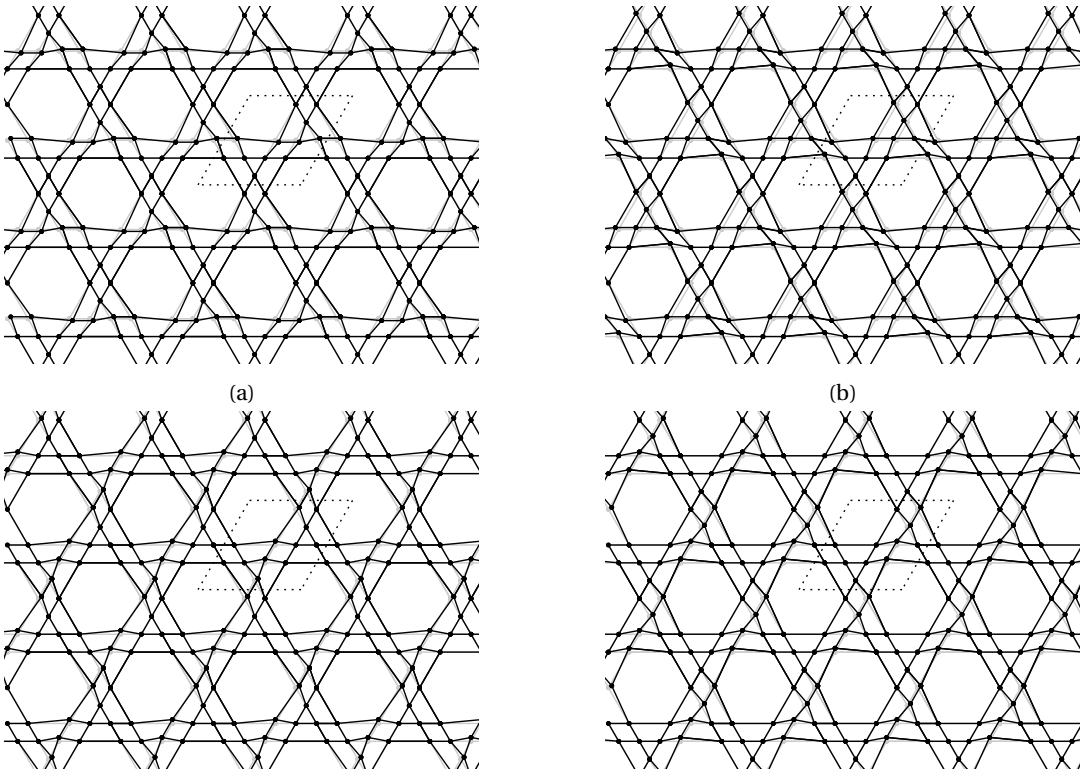

(a) (b) (c) (d)

Figure 4.3: The four non strain-producing linearised unit cell-periodic mechanisms of the DK micro-architecture.

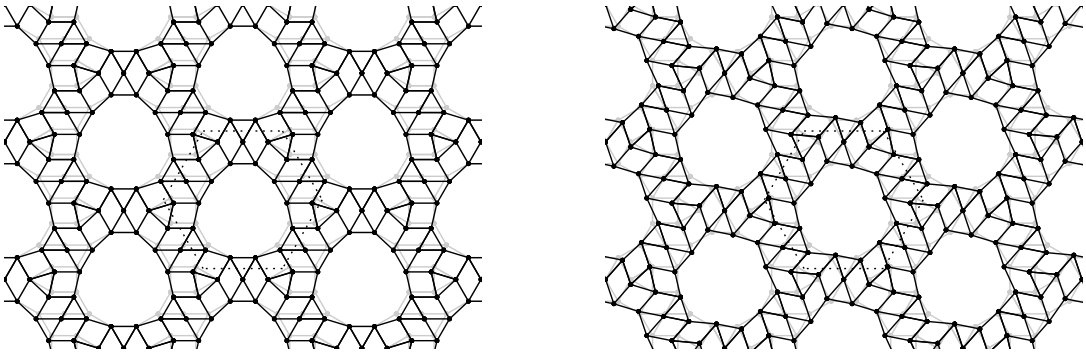

(a) (b)

Figure 4.4: The two non strain-producing linearised unit cell-periodic finite mechanisms of the MD micro-architecture.

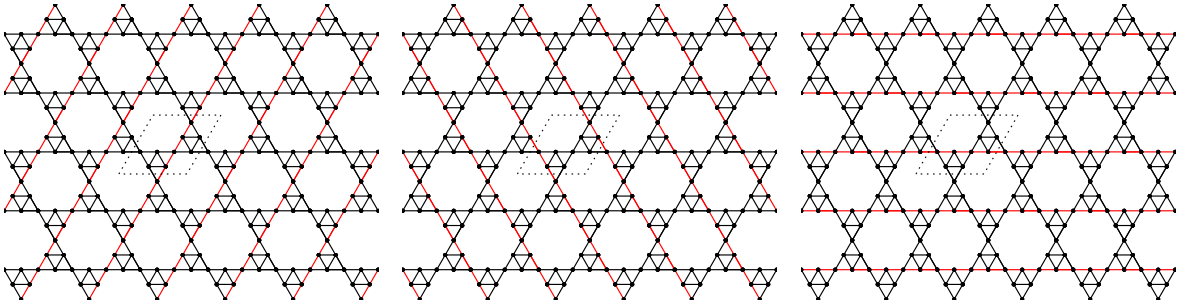

(a) (b) (c)

Figure 4.5: The three linearly independent states of self-stress of the KT structure. Red members sustain (unity) tension, black struts are tension-free.

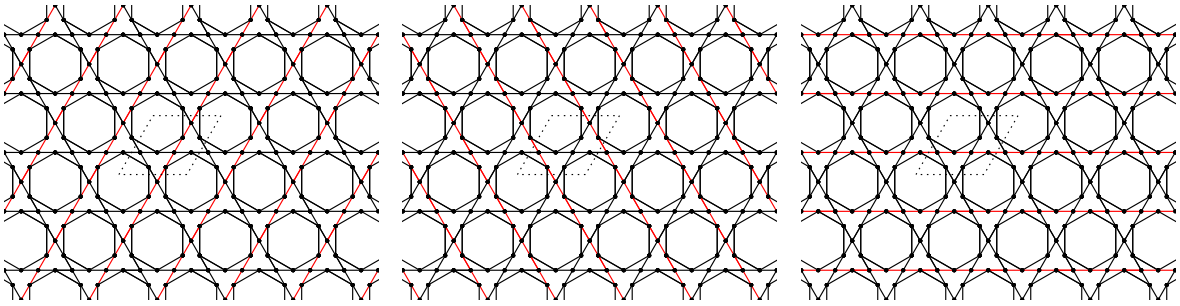

(a) (b) (c)

Figure 4.6: The three linearly independent states of self-stress of the KH structure. Red members sustain (unity) tension, black struts are tension-free.

contains all possible states of self-stress, i.e. all combinations of bar tensions that are in equilibrium with zero nodal loads. Each of these three states of self-stress is characterised by a set of aligned members sustaining the same (magnitude and sense) tension. The first and second states of self-stress concern members that are rotated with respect to the x_1-axis by 60°, clockwise and anti-clockwise, respectively. They are illustrated in Figs. 4.5a and 4.5b. The third vector in null($\boldsymbol{A}$) involves members that are oriented parallel to the x_1-direction, see Fig. 4.5c. The method of sections can be used to relate combinations of these states of self-stress to macroscopic stress states, see for instance [13]. The states listed in Eq. (4.7)/depicted in Fig. 4.5 evaluate to:

State 1 + State 2 - $\frac{1}{2}$State 3: $\quad \Sigma_{22} \neq 0, \quad \Sigma_{11} = \Sigma_{12} = 0,$

State 1 - State 2: $\quad \Sigma_{12} \neq 0, \quad \Sigma_{11} = \Sigma_{22} = 0,$

State 3: $\quad \Sigma_{11} \neq 0, \quad \Sigma_{12} = \Sigma_{22} = 0.$

Clearly, the pin-jointed KT structure can support all three linearly independent states of macroscopic stress. The KH structure has very similar states of self-stress (null($\boldsymbol{A}$) is listed in Appendix B), which are visualised in Fig. 4.6. Thus, rigid-jointed lattices with either of these architectures can sustain any macroscopic load without having members endure a significant bending load. This adds to the likeliness that lattice materials with these structure will show stretching-dominated deformation behaviour. Still, a part of the members, namely those that form the 'internal' triangles c.q. hexagons, are not stressed in any of the stress states shown in Figs. 4.5 and 4.6. This leads to the expectation that, also in rigid-jointed lattice materials with these micro-architectures, the internal members will not contribute significantly to the macroscopic stiffness. Therefore, sub-optimal elastic properties are expected for lattice materials with either of these micro-architectures.

The DK structure is capable of six linearly independent states of self stress; $s = 6$. They are found in the nullspace of $\boldsymbol{A}$, which is listed in Appendix B. Following the adopted definition [11], this structure is statically indeterminate, or redundant. Looking closer at the states of self-stress depicted in Fig. 4.7, each of them involves a (different) set of aligned members, similar to the previous structures. In fact, the DK truss has two states of self-stress that evaluate to the same macroscopic stress, where there is only one for the other designs. For example, consider Figs. 4.7b and e; while these states of self-stress differ as they involve different

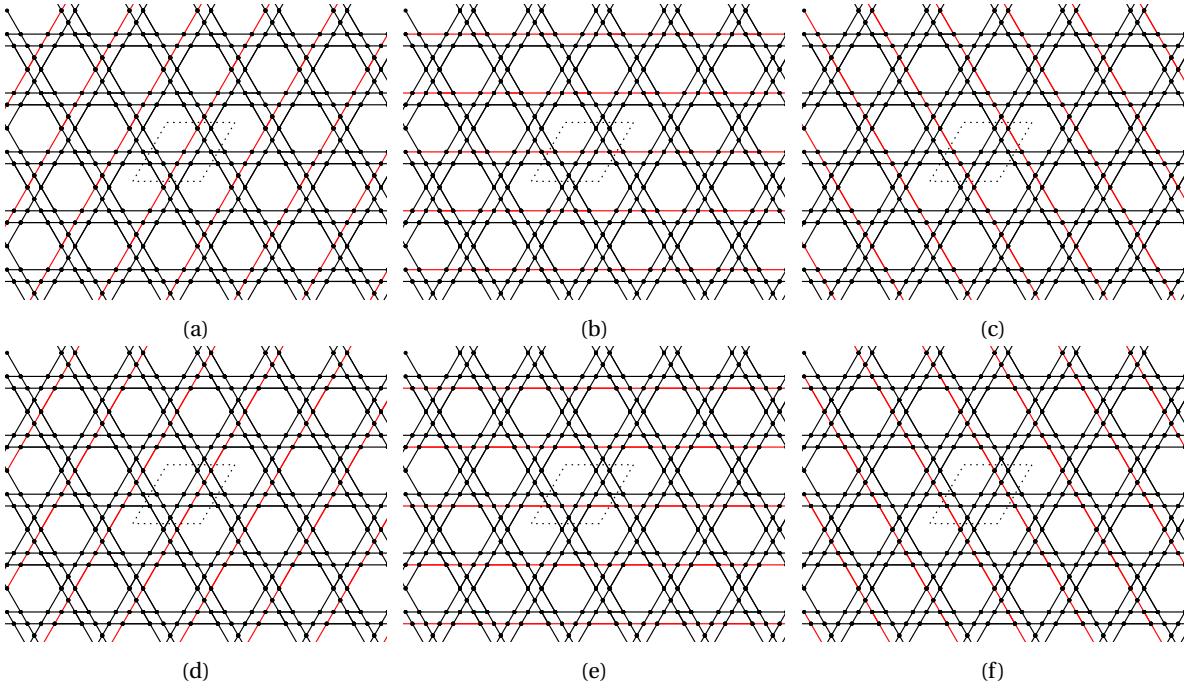

Figure 4.7: The six linearly independent states of self stress of the Double Kagome structure. Red members sustain (unity) tension, black struts are tension-free.

members, they evaluate to the same macroscopic stress if the method of sections is applied. Namely, $\Sigma_{11} \neq 0, \Sigma_{22} = \Sigma_{12} = 0$. Note that, upon summing all the stress states in Fig. 4.7, not only are all members in the truss loaded but also the bar tensions are equal. This indicates optimal use of material; like Kagome-structured materials, DK lattice material should have high elastic moduli.

The MD structure is topologically unrelated to any of the other structures. It has four possible linearly independent states of self-stress which are visualised in Fig. 4.8. The nullspace of the equilibrium matrix $\boldsymbol{A}$ is listed in Appendix B. While there are three stress-states that altogether evaluate to all possible planar macroscopic stresses (Figs. 4.8a, 4.8b and 4.8c), the magnitude of the bar tension differs between members. Colours indicate the different levels of bar force per the legend shown. Additionally, in contrast to the other structures, the fourth stress-state of the MD truss illustrated in Fig. 4.8d is of a different nature than the other three. The method of sections connects it to a biaxial macroscopic stress state: $\Sigma_{11} = \Sigma_{22} \neq 0,\ \Sigma_{12} = 0$. The varying levels of stress between the members most straightforwardly affect the strength of a lattice with this structure. The most heavily stressed members will fail prior to others (either by yielding or buckling), clearly resulting in a non-optimal overall yield strength.

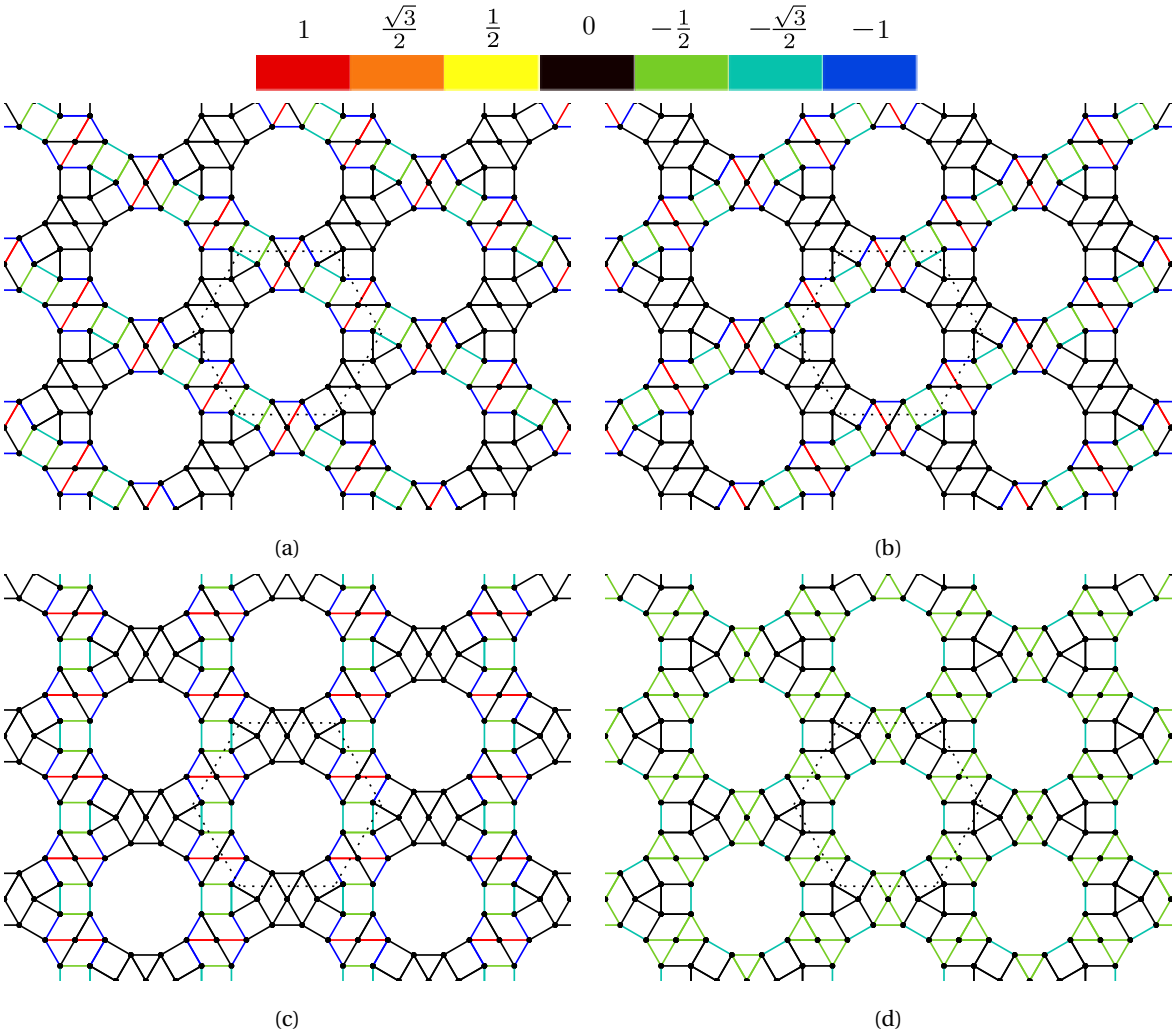

Figure 4.8: The four linearly independent states of self-stress of the MD structure. (a)-(c) are very similar and together evaluate to the three macroscopic stresses in 2D. The state of stress shown in (d) is of a different nature. Applying the method of sections links it to a biaxial macroscopic stress state. Colour indicates member tension per the legend shown above.

5

Mechanical characterisation

The initial (small strain) macroscopic mechanical response of 2D lattice materials is linear elastic and can therefore be characterised by effective elastic constants, see [27]. Since all the micro-architectures considered in this study are in-plane isotropic, two elastic moduli are sufficient to completely capture the linear-elastic material behaviour.

5.1. Models

The effective elastic properties of the different lattices were determined numerically using the finite element method. The commercial finite element program Abaqus (v6.14) was employed for these calculations. Each member of the unit cells was modelled using a single Timoshenko beam element (Abaqus element B22). All members have a rectangular cross-section with in-plane bar width w and a constant out-of-plane thickness. Linear elastic material behaviour is assumed for the base material, with Young's modulus E_s and Poisson's ratio ν_s. A representative unit cell with periodic boundary conditions mimics the behaviour of an infinitely large lattice. A clear account of how to determine the appropriate boundary conditions for a certain combination of structure and load is presented by Li [18]. Appendix C summarises the derivation of boundary conditions for symmetric rectangular 2D unit cells under uniaxial strain. Geometric linearity is assumed; the models are restricted to small strains.

Calculations of the properties of the Kagome lattice are included for comparison: Hyun and Torquato [15] showed that, in the limit $\bar{\rho} \to 0$, the Kagome lattice attains the Hashin-Shtrikman upper bounds on the bulk and shear modulus [12]. In other words, for low values of $\bar{\rho}$, deformation of the Kagome lattice is completely stretching-dominated.

Fig. 5.1 shows the geometries used for FE analysis of each of the structures. All of them represent one-fourth of a rectangular unit cell of the respective structure. Each of the indicated boundaries (dashed or dash-dotted) is a line of symmetry of a (different) representative translational unit cell. The left and bottom boundaries were chosen as symmetry lines for the application of boundary conditions in the FE models, therefore they are shown dash-dotted.

The cells shown in Figs. 5.1a - d are of equal size: $w_c \times h_c = l_0 \times l_0\sqrt{3}$. The members of the Kagome structure each have length l_0, as do the members of the MD structure. This causes the FE cell of the latter to have dimensions $(3+\sqrt{3})l_0 \times (1+\sqrt{3})l_0$. It is depicted in Fig. 5.1e. Expressions for the relative densities of all structures considered here are listed in Table 5.1. The MD structure is the lightest for a fixed width-to-length ratio w/l_0, followed (in order) by Kagome, KT, KH and DK.

For relative densities $\bar{\rho} \geq 0.15$, the slenderness ratio of members drops below 10 for some structures. As beam theory quickly becomes less accurate at lower slenderness ratios, calculations up to $\bar{\rho} = 0.15$ are deemed appropriate. The KT micro-architecture has the lowest slenderness at any value of $\bar{\rho}$, for this structure the limits of beam theory are encountered first.

Deformation is applied through imposed displacements of boundary nodes. Uniaxial tension/compression

Table 5.1: Relative densities of the considered structures as a function of in-plane bar width.

Structure	Kagome	KT	KH	DK	MD
$\bar{\rho}(w)$	$\sqrt{3}\frac{w}{l_0}$	$\frac{3}{2}\sqrt{3}\frac{w}{l_0}$	$(\sqrt{3}+\frac{3}{2})\frac{w}{l_0}$	$2\sqrt{3}\frac{w}{l_0}$	$\frac{21}{6+4\sqrt{3}}\frac{w}{l_0}$

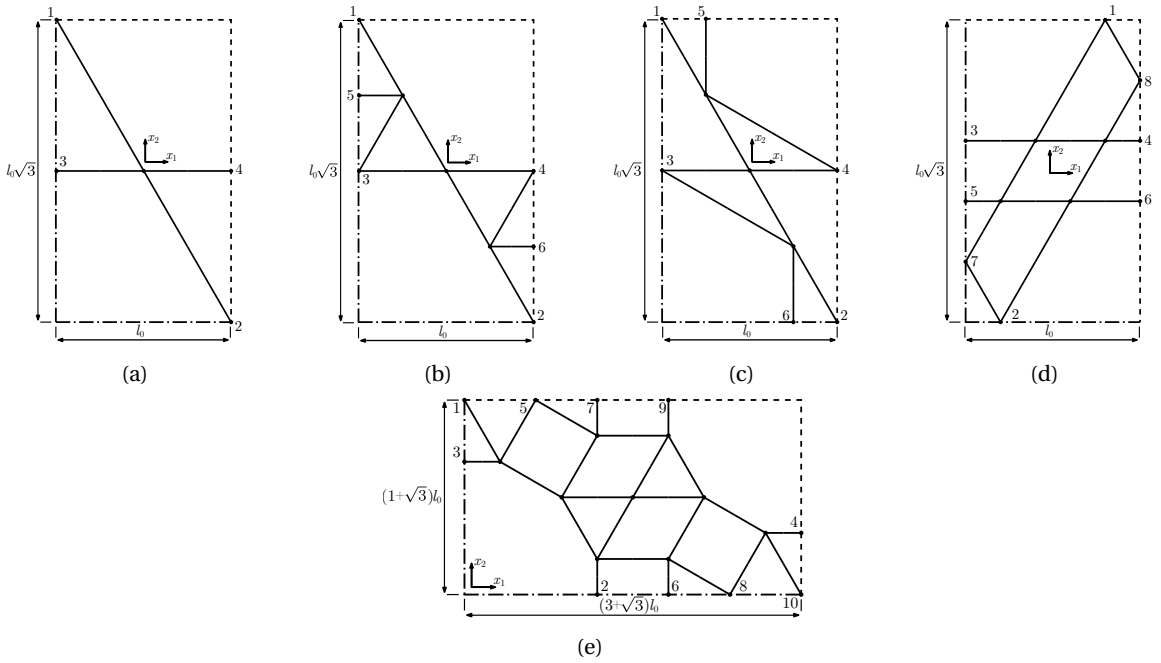

Figure 5.1: Geometries for FE analysis of lattice materials with the (a) Kagome, (b) KT, (c) KH, (d) DK and (e) MD structure. Dash-dotted symmetry lines used for application of boundary conditions are shown.

in the x_1-direction is simulated. Taking the Kagome structure as an example, the following sets of boundary conditions are established:

$$u_1^{(1)} = u_1^{(3)} = 0, \qquad u_2^{(2)} = 0, \qquad \varphi^{(1)} = \varphi^{(2)} = \varphi^{(3)} = 0, \tag{5.1a}$$

$$u_1^{(2)} = u_1^{(4)}, \qquad \varphi^{(4)} = 0, \tag{5.1b}$$

$$u_1^{(4)} - u_1^{(3)} = \varepsilon_{11}^* w_c, \tag{5.1c}$$

where $u_i^{(J)}$ and $\varphi^{(J)}$ denote the displacement in x_i direction and the in-plane rotation of node J, respectively. For the other structures, the conditions in Eq. (5.1a) apply to additional nodes that lie on the same line of symmetry. Periodicity/translational symmetry requires the symmetric cell to keep its rectangular shape after deformation. This is enforced through Eq. (5.1b). For structures that feature more than one node on the top boundary, a similar condition is applied equating all the x_2-displacements of those nodes. For example, in case of the MD structure: $d_2^{(1)} = d_2^{(5)} = d_2^{(7)} = d_2^{(9)}$.

The boundary condition in Eq. (5.1c) implicitly defines an effective strain measure for the x_1-direction. A similar expression is easily derived for strain in the x_2-direction:

$$\varepsilon_{11}^* = \frac{d_1^{(4)} - d_1^{(3)}}{w_c}, \quad \varepsilon_{22}^* = \frac{d_2^{(1)} - d_2^{(2)}}{h_c}. \tag{5.2}$$

Note that these strain measures are valid for all structures, if node numbering as seen in Fig. 5.1 is applied. With measures of strain in both the x_1- and x_2-direction defined, the macroscopic Poisson's ratio can be calculated;

$$\nu^* = -\frac{\varepsilon_{22}^*}{\varepsilon_{11}^*}, \tag{5.3}$$

valid when strain in the x_1-direction is imposed.

The effective stress resulting from the prescribed displacement is calculated using the undeformed cell dimensions. The reaction forces (in the principal direction of deformation) on the boundary nodes where the strain displacements are prescribed are summed and divided by the boundary surface area in the undeformed configuration:

$$\sigma^*_{ij} = \frac{1}{A_j} \sum_{k=1}^{n} f_i^{(k)}, \tag{5.4}$$

where there are n nodes on the considered boundary. $f_i^{(k)}$ denotes the i-component of the reaction force on boundary node k. A_j is the surface area of the boundary with an outward normal in the x_j-direction. It is equal to the boundary length multiplied by the out-of-plane thickness.

Having defined measures of stress and strain, the effective Young's modulus for isotropic structures is simply:

$$E^* = \frac{\sigma^*_{11}}{\varepsilon^*_{11}} \tag{5.5}$$

which can be normalised with the properties of the solid base material:

$$\bar{E} = \frac{E^*}{E_s}. \tag{5.6}$$

5.2. Results

Fig. 5.2a shows the calculated normalised effective Young's moduli of the investigated structures as a function of relative density. Fig. 5.2b shows their Poisson's ratios. For each of the structures, $\bar{E}$ scales (nearly) linearly with $\bar{\rho}$, which is characteristic for stretching-dominated lattices. In terms of stiffness, the Kagome lattice is matched only by the DK structure. As anticipated based on the matrix analysis results, the DK micro-architecture yields the highest possible elastic moduli for an isotropic lattice material [15].

The KH and KT micro-architectures result in almost equal Young's moduli. This is surprising since at the same value of $\bar{\rho}$, the struts in a KT lattice material are $\sim 25\%$ wider than those in a KH lattice. Analysing the deformed unit cells of KT and KH micro-architectures reveals that larger transverse (i.e. bending) forces occur in KH lattice material members, especially with increasing density. This explains both the fact that E^* increases slightly more than linearly with $\bar{\rho}$ and that KH surpasses KT for $\bar{\rho} \geq 0.15$, as with increasing density the bending stiffness of struts increases relative to their axial stiffness. A brief analysis of deformed unit cells of the two structures can be found in Appendix D.

Since all considered structures feature axes of three-fold symmetry, each of them has in-plane isotropic mechanical properties. Because of this and the fact that linear elastic base material properties are assumed, the complete planar mechanical behaviour is captured by two effective elastic constants; E^* and ν^*, for instance. Each of the other (four) elastic moduli can be calculated using the appropriate relation. For example, the shear modulus is related to E and ν through:

$$G = \frac{E}{2(1+\nu)}. \tag{5.7}$$

The uniaxial strain FE results were verified using Eq. (5.7): An additional model was built for each of the structures, in which a simple shear deformation is applied. Similar to the calculation of E^* described earlier, G^* is determined numerically from these models. The results of these models, shown in Fig. 5.2c, are in perfect agreement with the values found when evaluating Eq. (5.7) for the E^* and ν^* data from the uniaxial compression models.

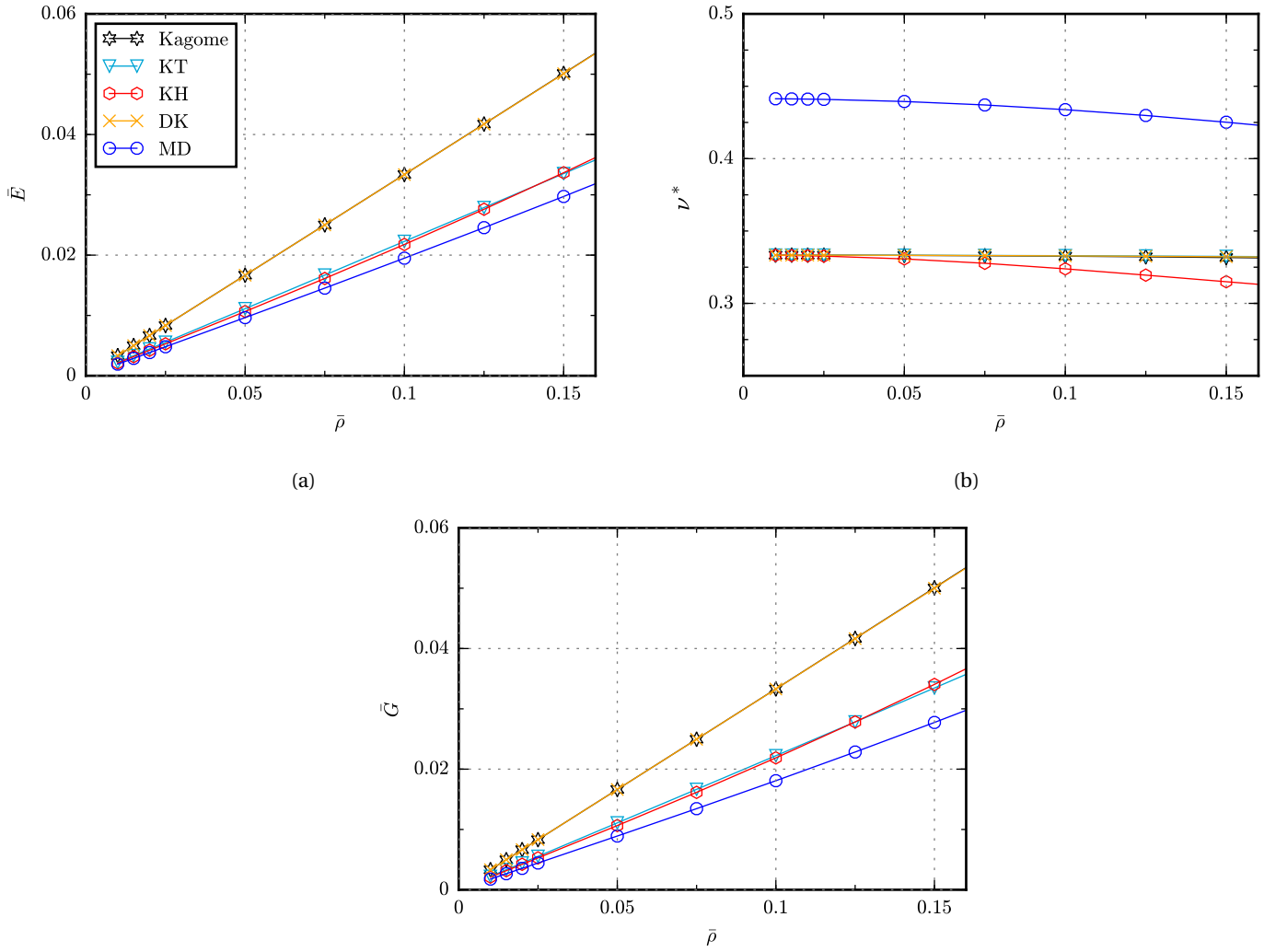

(a) (b)

(c)

Figure 5.2: (a) Normalised Young's modulus E^*/E_s, (b) Poisson's ratio and (c) normalised shear modulus G^*/G_s of the investigated micro-architectures as a function of relative density.

6

Single member actuation

The resistance of a lattice material to actuation was first quantified in Wicks and Guest [28] by the energy consumed by a single actuator replacing a regular member in the micro-architecture. If that actuator brings about an actuation strain ε_a, the required actuation energy is

$$W = -\frac{1}{2} t l \varepsilon_a, \tag{6.1}$$

where t is the tension in the member after actuation and l is the original member length. Note that this measure of energy is only valid assuming geometric linearity and linear elastic material behaviour. A reference energy W_0 is defined as a means to normalise and compare actuation energies of different structures; it is taken as the work performed by an actuator if it were surrounded by a rigid structure. In that case, the tension in the member after actuation is $t_0 = -E_s A \varepsilon_a$, resulting in

$$W_0 = \frac{1}{2} E_s A l \varepsilon_a^2. \tag{6.2}$$

The normalised actuation energy is defined as $\hat{W} = W/W_0$; a low value of $\hat{W}$ indicates an easily actuated micro-architecture.

For three lattices of distinct natures, how the actuation energy scales with member stockiness s is investigated in Wicks and Guest [28]. Stockiness, being the inverse of slenderness, is defined as the radius of gyration of a member divided by the member length: $s = k/l$. The radius of gyration k is a measure of the bending stiffness of a beam compared to its cross-sectional area. It is defined as $k = \sqrt{I/A}$, with I the second moment of area and A the area of the cross-section. Three cases were identified: for the statically indeterminate triangulated structure, $\hat{W}$ is (nearly) independent of s. For the kinematically indeterminate hexagonal micro-architecture, $\hat{W}$ scales with s^2. The Kagome structure yields a lattice material for which $\hat{W} \propto s^1$.

6.1. Models

Actuation energies have been calculated using models similar to those used in Wicks and Guest [28] and Pronk et al. [24]: the models represent rectangular sheets of lattice material, each strut of which is modelled using a single Euler-Bernoulli beam element (Abaqus element B23). Upper and lower bounds have been established: the upper bound being the value in case the boundary of the lattice is fixed, the lower bound is the value found with a free boundary. The former obviously constitutes a model that is stiffer than an infinitely large sheet of lattice material, therefore overestimating the actuation energy. Free boundary models on the other hand are over-compliant, resulting in an underestimate of the actuation energy. The sheets of lattice material modelled here are larger than those in just mentioned literature; approximately $800 l_0 \times 30 l_0 \sqrt{3}$. This is done to reduce the difference between the upper and lower bounds, especially at low values of $\bar{\rho}$ (see Figs. 4 and 8 in Wicks and Guest [28]).

Results presented here are for lattices comprising members with rectangular cross-sections. The in-plane bar width w is varied, while the out-of-plane thickness is maintained constant. Normalised actuation energies

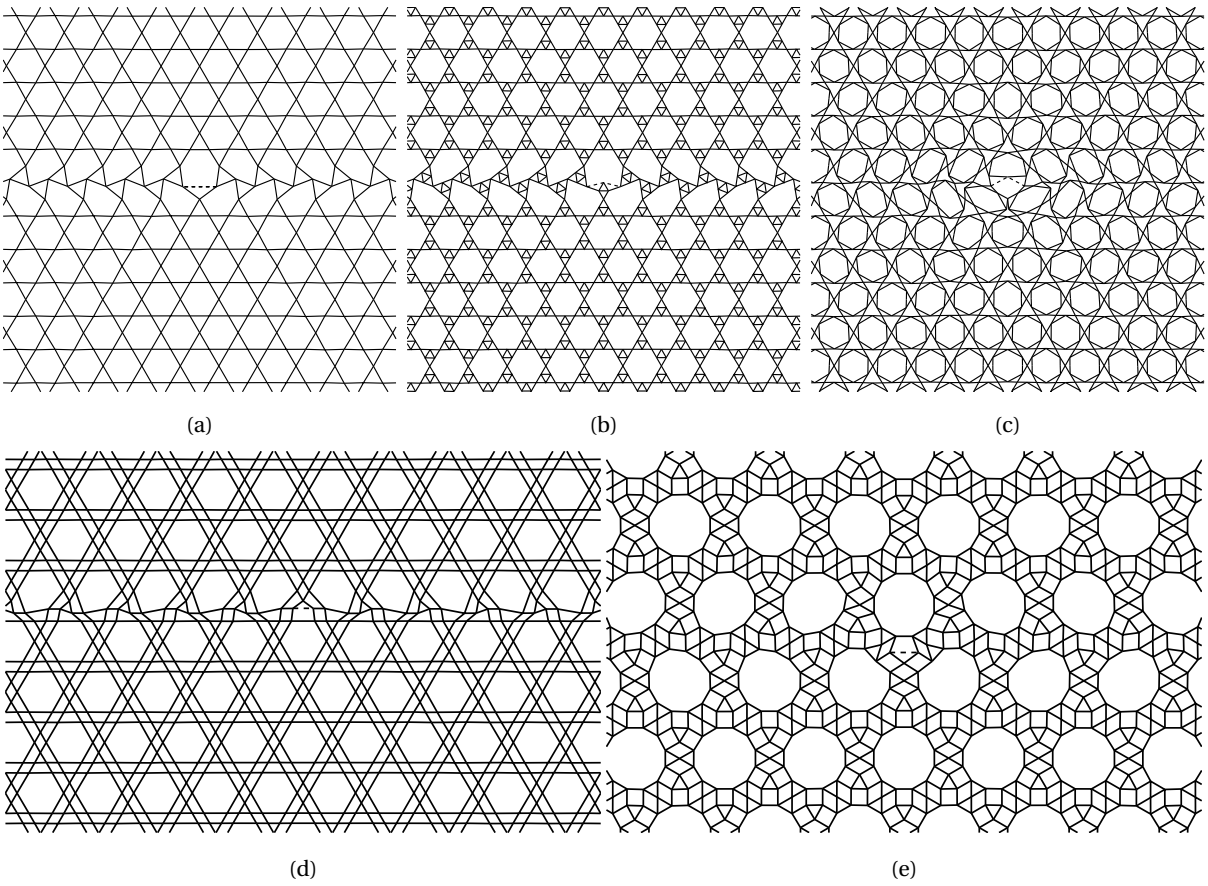

Figure 6.1: Center portions of five lattices after 'single member' actuation. (a): Kagome, (b): KT, (c) KH, (d): DK, (e): MD. Two members are actuated in the KT and KH lattices to achieve symmetric deformation, similar to the single member Kagome results. Displacements are greatly magnified, $\bar{\rho} = 0.01$.

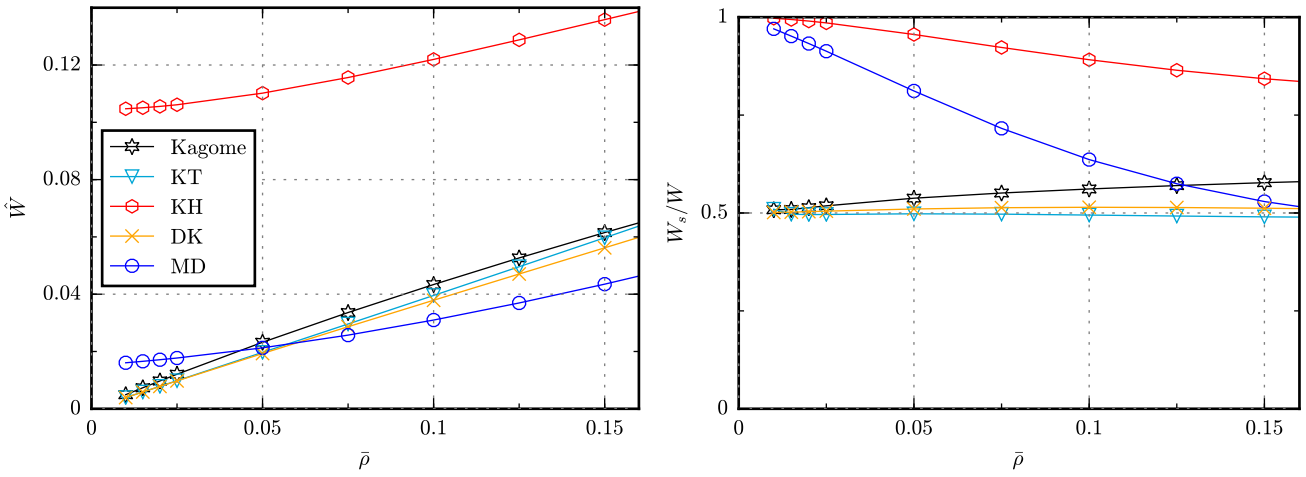

(a) (b)

Figure 6.2: Upper bound for (a) the normalised actuation energy $\hat{W} = W/W_0$ and (b) the fraction of the actuation energy stored by stretching of members.

are reported as a function of $\bar{\rho}$, so as to facilitate comparison of both mechanical and actuation properties in terms of the same parameter. Also, since some of the structures (KH, DK) contain members of different lengths, a certain value of w does not result in a single value of stockiness for all members.

Note that because of its high level of symmetry, actuation of any member of the Kagome micro-architecture is equivalent. The other designs contain more members that are not identical through symmetry; two kinds of members appear in KT and KH lattice material, three in DK and there are five different kinds of struts in the MD micro-architecture. Replaced by an actuator, each kind of strut constitutes a different mode of actuation. Based on preliminary actuation energy results, the most promising mode was selected for each of the designs. Those are illustrated in Fig. 6.1. Two members are replaced by actuators in the KT and KH structures, so that the effects of actuation are symmetric.

6.2. Results

Fig. 6.2a shows the normalised actuation energies for the investigated micro-architectures. Fig. 6.2b shows how the strain energy in the lattices is distributed between stretching and bending of members. The part stored by stretching is listed. For both quantities, the established upper and lower bounds are very close (within 5%), therefore only the upper bounds are listed.

It is interesting to see that all the considered micro-architectures except for the KH structure result in very similar values of $\hat{W}$. While the high actuation energy of the KH structure seems to be a logical consequence of stretching-dominated deformation (Fig. 6.2b), the MD structure surprises: at low values of $\bar{\rho}$, the MD lattice has a low actuation energy even though almost 100% of the energy is stored by stretching of members. This implies that only a limited number of struts is deformed due to the lengthening of the actuator and/or that the deformations are very small. At least it is clear that $\hat{W}$ is not simply related to $\hat{W}_s$.

Energy cost of actuation is not the only criterion for the selection of an actuation material: it is also interesting to quantify the effects of actuation. [28] noted that in a Kagome lattice "the distance over which deformation dies away depends on the stockiness.". The fact that the deformations are stockiness-dependent, and thus dependent on $\bar{\rho}$, actually explains the approximately linear dependency of $\hat{W}$ on $\bar{\rho}$.

As seen in Fig. 6.1, actuation effects differ greatly between lattice architectures. A Kagome and KT lattice show almost identical responses to actuation; lengthening of member(s) is accommodated by alternating rotations of opposed triangles. In the deformed DK lattice in Fig. 6.1d, similar rotations of triangles appear, but here only a single row of triangles is involved. Also, the triangles are not directly connected, requiring the displacements to be 'passed along' by deformation of the rhombi and trapeziums in between. In the actuated

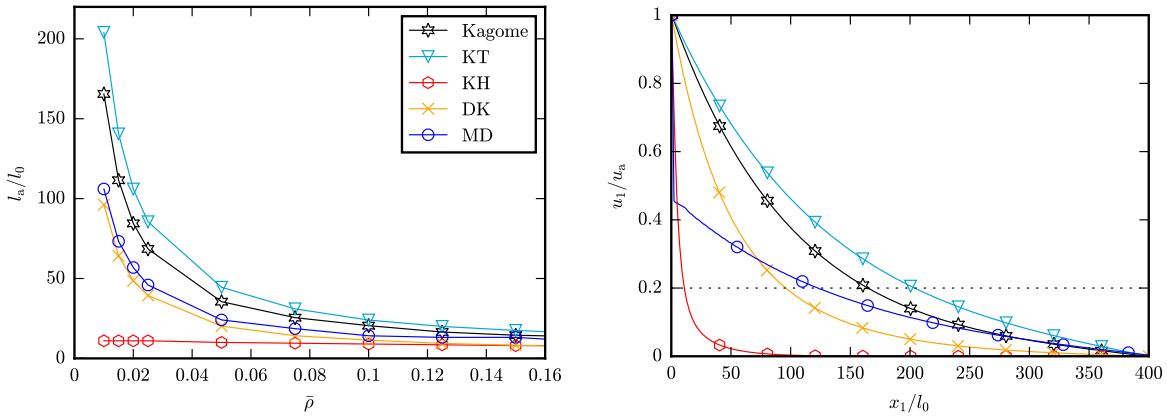

(a) (b)

Figure 6.3: Attenuation: (a) Attenuation distance as a fucntion of relative density. This graph shows the distance from the actuatior at which the displacements have damped out to 20% of the displacement of the actuated nodes. (b) Decay of displacements/deformations (in the direction of actuation) with distance from the actuator for $\bar{\rho} = 0.01$. Not all data points are marked to increase clarity. The dotted line indicates the 20%-displacement level of Fig. 6.3a.

MD lattice in Fig. 6.1e the affected 'corridor' is wider. Here too rotations of triangles and deformations of rhombi are apparent. The effects of actuation are very localised in the KH lattice in Fig. 6.1c. The structure is severely distorted in the direct vicinity of the actuator, but within the distance of a few unit cells the effects diminish to nearly nothing.

Fig. 6.3a shows attenuation distances plotted against $\bar{\rho}$ for all considered structures. Looking at members aligned with the actuator, attenuation distance is defined as the distance from the actuator at which the deformations, in the direction of actuation, have reduced to 20% of the displacement of the tip(s) of the actuator. Of course, the attenuation distance l_a decreases with increasing density for all structures. Fig. 6.3b shows exactly how the displacements attenuate with distance (to the right of the actuator) in case $\bar{\rho} = .01$.

Note that a low(er) actuation energy is not necessarily associated with a large(r) attenuation distance. Compare for instance the results of the Kagome, KT and DK structures. Still, deformations are limited to a very small region surrounding the actuator in the KH lattice, which has the highest actuation energy. The MD lattice shows very different attenuation behaviour than the other structures: after a large reduction (~ 60%) of the displacement magnitude within a small distance from the actuator, the deformations attenuate very gradually.

7

Discussion

All the results presented in this thesis are summarised in Table 7.1. The newly introduced micro-architectures satisfy Eq. (2.4), and therewith satisfy $s - m = 0$, their number of states of self-stress is equal to the number of non-strain producing displacement modes. Augmented matrix analysis verified that there are no strain-producing mechanisms associated with any of the structures: $ms = 0$. It was also shown that (linear combinations of) the states of self-stress can be linked to each of the three macroscopic stress-states that exist in 2D: $S = 3$. Table 7.1 also lists these properties for Kagome, Hexagonal Cupola and Triangulated lattice materials. Part of these results are collected from literature, see Wicks and Guest [28], Hutchinson and Fleck [13] and Pronk et al. [24]. Matrix analysis of the Triangulated structure is detailed in Appendix E.

Matrix analysis of periodic trusses with the KH and KT structure showed they have similar static and kinematic properties. In fact, their entries in Table 7.1 are identical. Also, they are equal to the values for the Kagome structure. In Chapter 5, lattices with the KH and KT structure were shown to perform very similarly in terms of macroscopic elastic properties. On the contrary, their actuation performances could not be further apart: first, Fig. 6.2a shows that a KH lattice by far has the highest actuation energy of all considered structures, while the KT structure is amongst the lowest. Secondly, regarding attenuation distance the KT and KH structures actually set the extremes (Fig. 6.3): deformation hardly spreads away from an actuator in a KH lattice, while it damps out the slowest in KT lattice material. The KH structure satisfies all of the criteria proposed by Pronk et al. [24]. With its poor actuation performance, the structure shows that the criteria do not guarantee favourable actuation characteristics.

The low and approximately linearly scaling actuation energies of DK and MD lattice materials are surprising as, according to the definition adopted here, these structures are statically indeterminate i.e. redundant; periodic pin-jointed trusses with the DK and MD micro-architecture have $s = 6$ and $s = 4$, respectively. Pronk et al. [24] proposed that for a lattice material architecture to be suitable for actuation, its pin-jointed truss version must be statically determinate per the definition for repetitive structures of Guest and Hutchinson [11]. The DK and MD micro-architectures prove by counterexample that this is an over-restrictive criterion.

It therewith also seems that the definition of static determinacy for infinite repetitive structures adopted here is not actually equivalent to its finite counterpart. A statically indeterminate repetitive truss with $s \geq 3$ namely is not necessarily redundant; analysis of the states of self-stress of the DK and MD structure in Chapter 4 showed that each of them is linked to macroscopic stress. That is, no set of members in these trusses can actually sustain a non-zero bar tension without the presence of a remote load.

For the range of $\bar{\rho}$ considered, Fig. 6.2a shows that DK lattice material has a lower actuation energy than a Kagome lattice. Also, looking at Fig. 5.2, both structures result in optimal [12] isotropic macroscopic elastic moduli at equal values of $\bar{\rho}$. The DK micro-architecture therewith is the first encountered structure that yields properties surpassing those of Kagome lattice material.

Actuation deformations do attenuate more quickly in a DK lattice according to the graphs in Fig. 6.3. Remember that the unit cells for Kagome and DK were assumed of the same shape and size; therefore members

Table 7.1: Properties of periodic trusses/rigid-jointed lattices with seven different micro-architectures.

	Micro-architecture(s)				
Property	Kagome KT KH	DK	MD	Triangulated	Hex. Cupola
s (Linearly independent states of self-stress)	3	6	4	6	3
S (Supported linearly independent macroscopic stress states)	3	3	3	3	1
m (Linearly independent non strain-producing displacement modes)	3	6	4	2	3
ms (Linearly independent strain-producing mechanisms)	0	0	0	0	2
Deformation behaviour	Stretching-dominated	Stretching-dominated	Stretching-dominated	Stretching-dominated	Bending-dominated
Actuation energy scaling	$\hat{W} \propto \bar{\rho}^1$	$\hat{W} \propto \bar{\rho}^1$	$\hat{W} \propto \bar{\rho}^1$	$\hat{W} \propto \bar{\rho}^0$	$\hat{W} \propto \bar{\rho}^2$

in DK lattice material are shorter. Compare Figs. 5.1a and d; the short and long members in the DK micro-architecture are 0.4× and 0.8× the length of Kagome members, respectively. It is likely that a minimal feature size would apply for the production of lattice materials with either of the two designs. If bar width were limiting at a given value of $\bar{\rho}$, the DK members' lengths, and therewith its unit cell dimensions, would be twice as large as assumed here. Given that the models are linear, the actuation deformations would attenuate over the same number of unit cells. Therewith, the attenuation distance of DK lattice material would also increase 2-fold and surpass Kagome's. If a minimal member length were to apply, the DK unit cell dimensions and attenuation distance would even scale by a factor 2.5.

8

Conclusion

The lattice material micro-architectures presented in this thesis allow for two main conclusions to be drawn.

First, there are designs that can compete with the Kagome architecture in terms of suitablilty for actuation. Three out of four proposed repetitive layouts comply with the simultaneous requirement of high, isotropic elastic moduli and limited resistance to actuation. They combine stretching-dominated deformation behaviour with linearly scaling actuation energy. The DK structure unprecedentedly outperforms Kagome, combining the same optimal isotropic elastic moduli with a lower actuation energy.

Secondly, the criteria for a lattice material to be suitable for actuation proposed by Pronk et al. [24] are over-restrictive: lattice materials with a statically indeterminate micro-architecture do not necessarily have a high actuation energy. Also, the criteria are not sufficient: one of the novel micro-architectures meets each of them, but results in large resistance to actuation. In addition, the effects of actuation are very localised.

9

Recommendations

This research has mainly shown that there are more 2D lattice material micro-architectures like the Kagome structure. While a lot of research has been done on lattice materials, some suggested research directions are listed here.

- The most thorough analysis of the statics and kinematics of periodic pin-jointed trusses is due to Hutchinson and Fleck [13]. In this study, Bloch's theorem is applied to develop a generalised matrix analysis. The described method not only yields an infinite structure's inextensional displacement modes and states of self-stress that are unit cell-periodic, but also those that have a wavelength of more than one unit cell. Possibly, this more advanced analysis could identify the intrinsic difference between the KH, KT and Kagome structure.

- A lot of research has been done on topology optimisation of mechanical metamaterials. Having an increasingly good understanding of why which lattice material micro-architectures are suitable for actuation in 2D, more clear topological criteria can be determined. Using these criteria, topology optimisation can be a powerful tool to identify more lattice materials for actuation. After starting with a search in 2D, three-dimensional micro-architectures may be looked for.

- This research was limited to lattice materials that feature planar isotropy. Isotropic materials are very useful and often the material of choice. Still, many cases can be thought of where isotropic material is not necessarily optimal. Most currently known anisotropic 2D lattice materials are stretching-dominated in particular directions, but show bending-dominated deformation behaviour in other directions. A square grid is an example of such a micro-architecture. While even these materials can be useful for certain applications, anisotropic lattice materials that do show stretching-dominated deformation behaviour in response to loads from any direction would also be very interesting.

- The calculations presented in this thesis are all geometrically linear and assume small strains. Clearly, there are limits to where these results are applicable. The pin-jointed truss version of the proposed structures possess non strain-producing mechanisms. Some of these linearised mechanisms represent an increment of a finite mechanism that in other increments is associated with macroscopic strain. If lattice materials with these micro-architectures were to endure finite strains, they will possibly become unstable. Non-linear analysis of the deformation of the proposed lattice materials can give insight in how the instability will come into play.

- A large part of recent literature on mechanical metamaterials is concerned with auxetics; materials with a negative Poisson's ratio. The periodic mechanisms of most of the presented micro-architectures effect negative equibiaxial strain when finite displacements are considered. Therefore, they may be of interest in this field of research.

- The effects of large strain actuation of Kagome lattices was studied in [17]. Resulting from large-strain actuation, buckling phenomena and distortion of the lattice cause severe degradation of compressive stiffness. Depending on whether the actuator stretches or contracts, the stiffness drop is sudden or

more gradual. The non-linear effects of actuation clearly cannot be neglected and are thus an interesting research direction.

A

Augmented compatibility matrices

KH:

$$\boldsymbol{B}_{\text{aug}} =$$

$$\left[\begin{array}{cccccccccccccccccccc:ccc}
\frac{1}{2} & \frac{\sqrt{3}}{2} & -\frac{1}{2} & -\frac{\sqrt{3}}{2} & 0 & 0 & 0 & 0 & 0 & 0 & 0 & 0 & 0 & 0 & 0 & 0 & 0 & 0 & 0 & 0 & 0 \\
-\frac{1}{2} & \frac{\sqrt{3}}{2} & 0 & 0 & \frac{1}{2} & -\frac{\sqrt{3}}{2} & 0 & 0 & 0 & 0 & 0 & 0 & 0 & 0 & 0 & 0 & 0 & 0 & 0 & 0 & 0 \\
0 & 0 & \frac{\sqrt{3}}{2} & \frac{1}{2} & 0 & 0 & 0 & 0 & -\frac{\sqrt{3}}{2} & -\frac{1}{2} & 0 & 0 & 0 & 0 & 0 & 0 & 0 & 0 & 0 & 0 & 0 \\
0 & 0 & \frac{1}{2} & \frac{\sqrt{3}}{2} & 0 & 0 & 0 & 0 & 0 & 0 & -\frac{1}{2} & -\frac{\sqrt{3}}{2} & 0 & 0 & 0 & 0 & 0 & 0 & 0 & 0 & 0 \\
0 & 0 & 0 & 0 & 0 & 0 & -1 & 0 & 1 & 0 & 0 & 0 & 0 & 0 & 0 & 0 & 0 & 0 & 0 & 0 & 0 \\
0 & 0 & 0 & 0 & 0 & 0 & 0 & 0 & -1 & 0 & 1 & 0 & 0 & 0 & 0 & 0 & 0 & 0 & 0 & 0 & 0 \\
0 & 0 & 0 & 0 & 0 & 0 & 0 & 0 & 0 & 0 & -1 & 0 & 1 & 0 & 0 & 0 & 0 & 0 & 0 & 0 & 0 \\
0 & 0 & 0 & 0 & 0 & 0 & -\frac{1}{2} & \frac{\sqrt{3}}{2} & 0 & 0 & 0 & 0 & 0 & 0 & \frac{1}{2} & -\frac{\sqrt{3}}{2} & 0 & 0 & 0 & 0 & 0 \\
0 & 0 & 0 & 0 & 0 & 0 & 0 & 0 & 0 & 0 & \frac{1}{2} & \frac{\sqrt{3}}{2} & 0 & 0 & 0 & 0 & -\frac{1}{2} & -\frac{\sqrt{3}}{2} & 0 & 0 & 0 \\
0 & 0 & 0 & 0 & 0 & 0 & 0 & 0 & 0 & 0 & 0 & 0 & \frac{\sqrt{3}}{2} & \frac{1}{2} & 0 & 0 & -\frac{\sqrt{3}}{2} & -\frac{1}{2} & 0 & 0 & 0 \\
0 & 0 & 0 & -1 & 0 & 0 & 0 & 0 & 0 & 0 & 0 & 0 & 0 & 0 & 0 & 1 & 0 & 0 & 0 & \frac{1}{2} & 1 \\
\frac{1}{2} & -\frac{\sqrt{3}}{2} & 0 & 0 & 0 & 0 & 0 & 0 & 0 & 0 & 0 & 0 & 0 & 0 & -\frac{1}{2} & \frac{\sqrt{3}}{2} & 0 & 0 & -\frac{1}{4} & 0 & \frac{\sqrt{3}}{2} \\
-\frac{1}{2} & -\frac{\sqrt{3}}{2} & 0 & 0 & 0 & 0 & 0 & 0 & 0 & 0 & 0 & 0 & 0 & 0 & 0 & 0 & \frac{1}{2} & \frac{\sqrt{3}}{2} & \frac{1}{4} & \frac{\sqrt{3}}{2} & \frac{\sqrt{3}}{2} \\
0 & 0 & 0 & 0 & 0 & -1 & 0 & 0 & 0 & 0 & 0 & 0 & 0 & 0 & 0 & 0 & 0 & 1 & 0 & \frac{1}{2} & 1 \\
0 & 0 & 0 & 0 & -\frac{\sqrt{3}}{2} & \frac{1}{2} & 0 & 0 & \frac{\sqrt{3}}{2} & -\frac{1}{2} & 0 & 0 & 0 & 0 & 0 & 0 & 0 & 0 & \frac{\sqrt{3}}{2} & -\frac{1}{2} & 0 \\
0 & 0 & 0 & 0 & -\frac{1}{2} & \frac{\sqrt{3}}{2} & \frac{1}{2} & -\frac{\sqrt{3}}{2} & 0 & 0 & 0 & 0 & 0 & 0 & 0 & 0 & 0 & 0 & \frac{1}{2} & -\frac{\sqrt{3}}{2} & 0 \\
0 & 0 & 0 & 0 & 0 & 0 & 1 & 0 & 0 & 0 & 0 & 0 & -1 & 0 & 0 & 0 & 0 & 0 & 1 & 0 & 0 \\
0 & 0 & 0 & 0 & 0 & 0 & 0 & 0 & 0 & 0 & 0 & 0 & -\frac{\sqrt{3}}{2} & \frac{1}{2} & \frac{\sqrt{3}}{2} & -\frac{1}{2} & 0 & 0 & \frac{\sqrt{3}}{2} & -\frac{1}{2} & 0
\end{array}\right] \tag{A.1}$$

DK:

$$
\boldsymbol{B}_{\text{aug}} = \left[\begin{array}{cccccccccccccccccccccccc:ccc}
\frac{1}{2} & \frac{\sqrt{3}}{2} & 0 & 0 & 0 & 0 & 0 & 0 & -\frac{1}{2} & -\frac{\sqrt{3}}{2} & 0 & 0 & 0 & 0 & 0 & 0 & 0 & 0 & 0 & 0 & 0 & 0 & 0 & 0 & 0 & 0 & 0 \\
-\frac{1}{2} & \frac{\sqrt{3}}{2} & 0 & 0 & \frac{1}{2} & -\frac{\sqrt{3}}{2} & 0 & 0 & 0 & 0 & 0 & 0 & 0 & 0 & 0 & 0 & 0 & 0 & 0 & 0 & 0 & 0 & 0 & 0 & 0 & 0 & 0 \\
0 & 0 & \frac{1}{2} & \frac{\sqrt{3}}{2} & -\frac{1}{2} & -\frac{\sqrt{3}}{2} & 0 & 0 & 0 & 0 & 0 & 0 & 0 & 0 & 0 & 0 & 0 & 0 & 0 & 0 & 0 & 0 & 0 & 0 & 0 & 0 & 0 \\
0 & 0 & 0 & 0 & \frac{1}{2} & \frac{\sqrt{3}}{2} & 0 & 0 & 0 & 0 & -\frac{1}{2} & -\frac{\sqrt{3}}{2} & 0 & 0 & 0 & 0 & 0 & 0 & 0 & 0 & 0 & 0 & 0 & 0 & 0 & 0 & 0 \\
0 & 0 & 0 & 0 & -\frac{1}{2} & \frac{\sqrt{3}}{2} & 0 & 0 & 0 & 0 & 0 & 0 & \frac{1}{2} & -\frac{\sqrt{3}}{2} & 0 & 0 & 0 & 0 & 0 & 0 & 0 & 0 & 0 & 0 & 0 & 0 & 0 \\
0 & 0 & 0 & 0 & 0 & 0 & -1 & 0 & 1 & 0 & 0 & 0 & 0 & 0 & 0 & 0 & 0 & 0 & 0 & 0 & 0 & 0 & 0 & 0 & 0 & 0 & 0 \\
0 & 0 & 0 & 0 & 0 & 0 & 0 & 0 & -1 & 0 & 1 & 0 & 0 & 0 & 0 & 0 & 0 & 0 & 0 & 0 & 0 & 0 & 0 & 0 & 0 & 0 & 0 \\
0 & 0 & 0 & 0 & 0 & 0 & 0 & 0 & 0 & 0 & -1 & 0 & 1 & 0 & 0 & 0 & 0 & 0 & 0 & 0 & 0 & 0 & 0 & 0 & 0 & 0 & 0 \\
0 & 0 & 0 & 0 & 0 & 0 & -\frac{1}{2} & \frac{\sqrt{3}}{2} & 0 & 0 & 0 & 0 & 0 & 0 & 0 & 0 & \frac{1}{2} & -\frac{\sqrt{3}}{2} & 0 & 0 & 0 & 0 & 0 & 0 & 0 & 0 & 0 \\
0 & 0 & 0 & 0 & 0 & 0 & 0 & 0 & \frac{1}{2} & \frac{\sqrt{3}}{2} & 0 & 0 & 0 & 0 & 0 & 0 & 0 & 0 & -\frac{1}{2} & -\frac{\sqrt{3}}{2} & 0 & 0 & 0 & 0 & 0 & 0 & 0 \\
0 & 0 & 0 & 0 & 0 & 0 & 0 & 0 & 0 & 0 & \frac{1}{2} & \frac{\sqrt{3}}{2} & 0 & 0 & 0 & 0 & 0 & 0 & 0 & 0 & -\frac{1}{2} & -\frac{\sqrt{3}}{2} & 0 & 0 & 0 & 0 & 0 \\
0 & 0 & 0 & 0 & 0 & 0 & 0 & 0 & 0 & 0 & 0 & 0 & 0 & 0 & -1 & 0 & 1 & 0 & 0 & 0 & 0 & 0 & 0 & 0 & 0 & 0 & 0 \\
0 & 0 & 0 & 0 & 0 & 0 & 0 & 0 & 0 & 0 & 0 & 0 & 0 & 0 & 0 & 0 & -1 & 0 & 1 & 0 & 0 & 0 & 0 & 0 & 0 & 0 & 0 \\
0 & 0 & 0 & 0 & 0 & 0 & 0 & 0 & 0 & 0 & 0 & 0 & 0 & 0 & 0 & 0 & 0 & 0 & -1 & 0 & 1 & 0 & 0 & 0 & 0 & 0 & 0 \\
0 & 0 & 0 & 0 & 0 & 0 & 0 & 0 & 0 & 0 & 0 & 0 & 0 & 0 & 0 & 0 & -\frac{1}{2} & \frac{\sqrt{3}}{2} & 0 & 0 & 0 & 0 & \frac{1}{2} & -\frac{\sqrt{3}}{2} & 0 & 0 & 0 \\
0 & 0 & 0 & 0 & 0 & 0 & 0 & 0 & 0 & 0 & 0 & 0 & 0 & 0 & 0 & 0 & 0 & 0 & \frac{1}{2} & \frac{\sqrt{3}}{2} & 0 & 0 & -\frac{1}{2} & -\frac{\sqrt{3}}{2} & 0 & 0 & 0 \\
\frac{1}{2} & -\frac{\sqrt{3}}{2} & 0 & 0 & 0 & 0 & 0 & 0 & 0 & 0 & 0 & 0 & 0 & 0 & -\frac{1}{2} & \frac{\sqrt{3}}{2} & 0 & 0 & 0 & 0 & 0 & 0 & 0 & 0 & -\frac{1}{4} & -\frac{1}{4} & \frac{\sqrt{3}}{2} \\
-\frac{1}{2} & -\frac{\sqrt{3}}{2} & 0 & 0 & 0 & 0 & 0 & 0 & 0 & 0 & 0 & 0 & 0 & 0 & 0 & 0 & 0 & 0 & 0 & 0 & 0 & 0 & \frac{1}{2} & \frac{\sqrt{3}}{2} & \frac{1}{4} & \frac{\sqrt{3}}{2} & \frac{\sqrt{3}}{2} \\
0 & 0 & \frac{1}{2} & -\frac{\sqrt{3}}{2} & 0 & 0 & 0 & 0 & 0 & 0 & 0 & 0 & 0 & 0 & 0 & 0 & 0 & 0 & 0 & 0 & 0 & 0 & -\frac{1}{2} & \frac{\sqrt{3}}{2} & -\frac{1}{4} & 0 & \frac{\sqrt{3}}{2} \\
0 & 0 & -\frac{1}{2} & -\frac{\sqrt{3}}{2} & 0 & 0 & 0 & 0 & 0 & 0 & 0 & 0 & 0 & 0 & 0 & 0 & 0 & 0 & 0 & 0 & \frac{1}{2} & \frac{\sqrt{3}}{2} & 0 & 0 & \frac{1}{4} & \frac{\sqrt{3}}{2} & \frac{\sqrt{3}}{2} \\
0 & 0 & -\frac{1}{2} & \frac{\sqrt{3}}{2} & 0 & 0 & \frac{1}{2} & -\frac{\sqrt{3}}{2} & 0 & 0 & 0 & 0 & 0 & 0 & 0 & 0 & 0 & 0 & 0 & 0 & 0 & 0 & 0 & 0 & \frac{1}{2} & -\frac{\sqrt{3}}{2} & 0 \\
0 & 0 & 0 & 0 & 0 & 0 & 1 & 0 & 0 & 0 & 0 & 0 & -1 & 0 & 0 & 0 & 0 & 0 & 0 & 0 & 0 & 0 & 0 & 0 & 1 & 0 & 0 \\
0 & 0 & 0 & 0 & 0 & 0 & 0 & 0 & 0 & 0 & 0 & 0 & -\frac{1}{2} & \frac{\sqrt{3}}{2} & \frac{1}{2} & -\frac{\sqrt{3}}{2} & 0 & 0 & 0 & 0 & 0 & 0 & 0 & 0 & \frac{1}{2} & -\frac{\sqrt{3}}{2} & 0 \\
0 & 0 & 0 & 0 & 0 & 0 & 0 & 0 & 0 & 0 & 0 & 0 & 0 & 0 & 1 & 0 & 0 & 0 & 0 & 0 & -1 & 0 & 0 & 0 & 1 & 0 & 0
\end{array}\right] \tag{A.2}
$$

MD:

$$\boldsymbol{B}_{\text{aug}} = \left[\begin{array}{cccccccccccccccccccccccccccccccccccccccccc|ccc}
\frac{\sqrt{3}}{2}&\frac{1}{2}&0&0&0&0&-\frac{\sqrt{3}}{2}&-\frac{1}{2}&0&0&0&0&0&0&0&0&0&0&0&0&0&0&0&0&0&0&0&0&0&0&0&0&0&0&0&0&0&0&0&0&0&0&0&0&0 \\
-\frac{1}{2}&\frac{\sqrt{3}}{2}&0&0&0&0&0&0&0&0&\frac{1}{2}&-\frac{\sqrt{3}}{2}&0&0&0&0&0&0&0&0&0&0&0&0&0&0&0&0&0&0&0&0&0&0&0&0&0&0&0&0&0&0&0&0&0 \\
0&0&\frac{1}{2}&\frac{\sqrt{3}}{2}&0&0&0&0&0&0&-\frac{1}{2}&-\frac{\sqrt{3}}{2}&0&0&0&0&0&0&0&0&0&0&0&0&0&0&0&0&0&0&0&0&0&0&0&0&0&0&0&0&0&0&0&0&0 \\
0&0&-\frac{1}{2}&\frac{\sqrt{3}}{2}&0&0&0&0&0&0&0&0&\frac{1}{2}&-\frac{\sqrt{3}}{2}&0&0&0&0&0&0&0&0&0&0&0&0&0&0&0&0&0&0&0&0&0&0&0&0&0&0&0&0&0&0&0 \\
0&0&0&0&-\frac{\sqrt{3}}{2}&\frac{1}{2}&0&0&\frac{\sqrt{3}}{2}&-\frac{1}{2}&0&0&0&0&0&0&0&0&0&0&0&0&0&0&0&0&0&0&0&0&0&0&0&0&0&0&0&0&0&0&0&0&0&0&0 \\
0&0&0&0&\frac{1}{2}&\frac{\sqrt{3}}{2}&0&0&0&0&0&0&-\frac{1}{2}&-\frac{\sqrt{3}}{2}&0&0&0&0&0&0&0&0&0&0&0&0&0&0&0&0&0&0&0&0&0&0&0&0&0&0&0&0&0&0&0 \\
0&0&0&0&0&0&-\frac{1}{2}&\frac{\sqrt{3}}{2}&0&0&0&0&0&0&0&0&\frac{1}{2}&-\frac{\sqrt{3}}{2}&0&0&0&0&0&0&0&0&0&0&0&0&0&0&0&0&0&0&0&0&0&0&0&0&0&0&0 \\
0&0&0&0&0&0&0&0&\frac{1}{2}&\frac{\sqrt{3}}{2}&0&0&0&0&0&0&0&0&-\frac{1}{2}&-\frac{\sqrt{3}}{2}&0&0&0&0&0&0&0&0&0&0&0&0&0&0&0&0&0&0&0&0&0&0&0&0&0 \\
0&0&0&0&0&0&0&0&0&0&-1&0&1&0&0&0&0&0&0&0&0&0&0&0&0&0&0&0&0&0&0&0&0&0&0&0&0&0&0&0&0&0&0&0&0 \\
0&0&0&0&0&0&0&0&0&0&\frac{\sqrt{3}}{2}&\frac{1}{2}&0&0&0&0&-\frac{\sqrt{3}}{2}&-\frac{1}{2}&0&0&0&0&0&0&0&0&0&0&0&0&0&0&0&0&0&0&0&0&0&0&0&0&0&0&0 \\
0&0&0&0&0&0&0&0&0&0&0&0&-\frac{\sqrt{3}}{2}&\frac{1}{2}&0&0&0&0&\frac{\sqrt{3}}{2}&-\frac{1}{2}&0&0&0&0&0&0&0&0&0&0&0&0&0&0&0&0&0&0&0&0&0&0&0&0&0 \\
0&0&0&0&0&0&0&0&0&0&0&0&0&0&-1&0&1&0&0&0&0&0&0&0&0&0&0&0&0&0&0&0&0&0&0&0&0&0&0&0&0&0&0&0&0 \\
0&0&0&0&0&0&0&0&0&0&0&0&0&0&-\frac{1}{2}&\frac{\sqrt{3}}{2}&0&0&0&0&0&0&0&0&\frac{1}{2}&-\frac{\sqrt{3}}{2}&0&0&0&0&0&0&0&0&0&0&0&0&0&0&0&0&0&0&0 \\
0&0&0&0&0&0&0&0&0&0&0&0&0&0&0&0&\frac{1}{2}&\frac{\sqrt{3}}{2}&0&0&0&0&0&0&-\frac{1}{2}&-\frac{\sqrt{3}}{2}&0&0&0&0&0&0&0&0&0&0&0&0&0&0&0&0&0&0&0 \\
0&0&0&0&0&0&0&0&0&0&0&0&0&0&0&0&0&0&-1&0&1&0&0&0&0&0&0&0&0&0&0&0&0&0&0&0&0&0&0&0&0&0&0&0&0 \\
0&0&0&0&0&0&0&0&0&0&0&0&0&0&0&0&0&0&-\frac{1}{2}&\frac{\sqrt{3}}{2}&0&0&0&0&0&0&\frac{1}{2}&-\frac{\sqrt{3}}{2}&0&0&0&0&0&0&0&0&0&0&0&0&0&0&0&0&0 \\
0&0&0&0&0&0&0&0&0&0&0&0&0&0&0&0&0&0&0&0&\frac{1}{2}&\frac{\sqrt{3}}{2}&0&0&0&0&-\frac{1}{2}&-\frac{\sqrt{3}}{2}&0&0&0&0&0&0&0&0&0&0&0&0&0&0&0&0&0 \\
0&0&0&0&0&0&0&0&0&0&0&0&0&0&0&0&0&0&0&0&0&0&-1&0&1&0&0&0&0&0&0&0&0&0&0&0&0&0&0&0&0&0&0&0&0 \\
0&0&0&0&0&0&0&0&0&0&0&0&0&0&0&0&0&0&0&0&0&0&0&0&0&1&0&0&0&0&0&-1&0&0&0&0&0&0&0&0&0&0&0&0&0 \\
0&0&0&0&0&0&0&0&0&0&0&0&0&0&0&0&0&0&0&0&0&0&0&0&0&0&-1&0&1&0&0&0&0&0&0&0&0&0&0&0&0&0&0&0&0 \\
0&0&0&0&0&0&0&0&0&0&0&0&0&0&0&0&0&0&0&0&0&0&0&0&0&0&0&1&0&0&0&0&0&-1&0&0&0&0&0&0&0&0&0&0&0 \\
0&0&0&0&0&0&0&0&0&0&0&0&0&0&0&0&0&0&0&0&0&0&0&0&0&0&0&0&0&0&-\frac{1}{2}&\frac{\sqrt{3}}{2}&0&0&\frac{1}{2}&-\frac{\sqrt{3}}{2}&0&0&0&0&0&0&0&0&0 \\
0&0&0&0&0&0&0&0&0&0&0&0&0&0&0&0&0&0&0&0&0&0&0&0&0&0&0&0&0&0&0&0&\frac{1}{2}&\frac{\sqrt{3}}{2}&0&0&-\frac{1}{2}&-\frac{\sqrt{3}}{2}&0&0&0&0&0&0&0 \\
0&0&0&0&0&0&0&0&0&0&0&0&0&0&0&0&0&0&0&0&0&0&0&0&0&0&0&0&0&0&0&0&0&0&-\frac{\sqrt{3}}{2}&\frac{1}{2}&0&0&\frac{\sqrt{3}}{2}&-\frac{1}{2}&0&0&0&0&0 \\
0&0&0&0&0&0&0&0&0&0&0&0&0&0&0&0&0&0&0&0&0&0&0&0&0&0&0&0&0&0&0&0&0&0&0&0&\frac{\sqrt{3}}{2}&\frac{1}{2}&0&0&-\frac{\sqrt{3}}{2}&-\frac{1}{2}&0&0&0 \\
0&0&0&0&0&0&0&0&0&0&0&0&0&0&0&0&0&0&0&0&0&0&0&0&0&0&0&0&0&0&0&0&0&0&0&0&0&0&-1&0&1&0&0&0&0 \\
-\frac{1}{2}&-\frac{\sqrt{3}}{2}&0&0&0&0&0&0&0&0&0&0&0&0&0&0&0&0&0&0&0&0&0&0&0&0&0&0&0&0&0&0&0&0&0&0&0&0&\frac{1}{2}&\frac{\sqrt{3}}{2}&0&0&0&\frac{\sqrt{3}}{3}&\sqrt{3} \\
0&0&\frac{1}{2}&-\frac{\sqrt{3}}{2}&0&0&0&0&0&0&0&0&0&0&0&0&0&0&0&0&0&0&0&0&0&0&0&0&0&0&0&0&0&0&0&0&0&0&-\frac{1}{2}&\frac{\sqrt{3}}{2}&0&0&0&-\frac{\sqrt{3}}{3}&\sqrt{3} \\
0&0&-\frac{1}{2}&-\frac{\sqrt{3}}{2}&0&0&0&0&0&0&0&0&0&0&0&0&0&0&0&0&0&0&0&0&0&0&0&0&0&0&0&0&0&0&0&0&0&0&0&0&\frac{1}{2}&\frac{\sqrt{3}}{2}&0&\frac{\sqrt{3}}{3}&\sqrt{3} \\
0&0&0&0&\frac{1}{2}&-\frac{\sqrt{3}}{2}&0&0&0&0&0&0&0&0&0&0&0&0&0&0&0&0&0&0&0&0&0&0&0&0&0&0&0&0&0&0&0&0&0&0&-\frac{1}{2}&\frac{\sqrt{3}}{2}&0&-\frac{\sqrt{3}}{3}&\sqrt{3} \\
0&0&0&0&-\frac{\sqrt{3}}{2}&-\frac{1}{2}&0&0&0&0&0&0&0&0&0&0&0&0&0&0&0&0&\frac{\sqrt{3}}{2}&\frac{1}{2}&0&0&0&0&0&0&0&0&0&0&0&0&0&0&0&0&0&0&\frac{\sqrt{3}}{2}&\frac{2\sqrt{3}}{3}&\frac{1}{2} \\
0&0&0&0&0&0&0&0&0&-1&0&0&0&0&0&0&0&0&0&0&0&0&0&1&0&0&0&0&0&0&0&0&0&0&0&0&0&0&0&0&0&0&0&\frac{\sqrt{3}}{3}&1 \\
0&0&0&0&0&0&0&0&-1&0&0&0&0&0&0&0&0&0&0&0&0&0&0&0&0&0&0&0&0&0&1&0&0&0&0&0&0&0&0&0&0&0&1&1&0 \\
0&0&0&0&0&0&0&0&0&0&0&0&0&0&0&0&0&0&0&0&-\frac{1}{2}&-\frac{\sqrt{3}}{2}&0&0&0&0&0&0&0&0&\frac{1}{2}&\frac{\sqrt{3}}{2}&0&0&0&0&0&0&0&0&0&0&\frac{1}{2}&1&\frac{\sqrt{3}}{2} \\
0&0&0&0&0&0&0&0&0&0&0&0&0&0&0&0&0&0&0&0&-1&0&0&0&0&0&0&0&0&0&0&0&0&0&1&0&0&0&0&0&0&0&1&1&0 \\
0&0&0&0&0&0&0&0&0&0&0&0&0&0&0&0&0&0&0&0&0&0&0&0&0&0&0&0&-\frac{1}{2}&-\frac{\sqrt{3}}{2}&0&0&0&0&\frac{1}{2}&\frac{\sqrt{3}}{2}&0&0&0&0&0&0&\frac{1}{2}&1&\frac{\sqrt{3}}{2} \\
\frac{\sqrt{3}}{2}&-\frac{1}{2}&0&0&0&0&0&0&0&0&0&0&0&0&0&0&0&0&0&0&0&0&0&0&0&0&0&0&-\frac{\sqrt{3}}{2}&\frac{1}{2}&0&0&0&0&0&0&0&0&0&0&0&0&\frac{\sqrt{3}}{2}&-1&\frac{1}{2} \\
0&0&0&0&0&0&0&-1&0&0&0&0&0&0&0&0&0&0&0&0&0&0&0&0&0&0&0&0&0&1&0&0&0&0&0&0&0&0&0&0&0&0&0&-1&1 \\
0&0&0&0&0&0&1&0&0&0&0&0&0&0&0&0&0&0&0&0&0&0&0&0&0&0&0&0&0&0&0&0&-1&0&0&0&0&0&0&0&0&0&1&-\frac{\sqrt{3}}{3}&0 \\
0&0&0&0&0&0&0&0&0&0&0&0&0&0&\frac{1}{2}&-\frac{\sqrt{3}}{2}&0&0&0&0&0&0&0&0&0&0&0&0&0&0&0&0&-\frac{1}{2}&\frac{\sqrt{3}}{2}&0&0&0&0&0&0&0&0&\frac{1}{2}&-\frac{2\sqrt{3}}{3}&\frac{\sqrt{3}}{2} \\
0&0&0&0&0&0&0&0&0&0&0&0&0&0&1&0&0&0&0&0&0&0&0&0&0&0&0&0&0&0&0&0&0&0&0&0&-1&0&0&0&0&0&1&-\frac{\sqrt{3}}{3}&0 \\
0&0&0&0&0&0&0&0&0&0&0&0&0&0&0&0&0&0&0&0&0&0&\frac{1}{2}&-\frac{\sqrt{3}}{2}&0&0&0&0&0&0&0&0&0&0&0&0&-\frac{1}{2}&\frac{\sqrt{3}}{2}&0&0&0&0&\frac{1}{2}&-\frac{2\sqrt{3}}{3}&\frac{\sqrt{3}}{2}
\end{array}\right] \qquad \text{(A.3)}$$

B

Nullspaces

KT:

$$\text{null}(\boldsymbol{A}) = \begin{bmatrix} 1 & 0 & 0 & 1 & 0 & 0 & 0 & 0 & 0 & 0 & 0 & 0 & 1 & 0 & 0 & 1 & 0 & 0 \\ 0 & 1 & 0 & 0 & 0 & 0 & 0 & 0 & 0 & 1 & 0 & 0 & 0 & 0 & 1 & 0 & 1 & 0 \\ 0 & 0 & 0 & 0 & 0 & 0 & 1 & 1 & 1 & 0 & 0 & 0 & 0 & 0 & 0 & 0 & 0 & 1 \end{bmatrix}^{\mathrm{T}} \tag{B.1}$$

$$\text{null}(\boldsymbol{B}_{\text{aug}}) = \begin{bmatrix} 0 & 1 & 0 & 1 & 0 & 1 & 0 & 1 & 0 & 1 & 0 & 1 & 0 & 1 & 0 & 1 & 0 & 1 & 0 & 0 & 0 \\ 1 & 0 & 1 & 0 & 1 & 0 & 1 & 0 & 1 & 0 & 1 & 0 & 1 & 0 & 1 & 0 & 1 & 0 & 0 & 0 & 0 \\ \sqrt{3} & -1 & \frac{\sqrt{3}}{2} & -\frac{1}{2} & \frac{\sqrt{3}}{2} & -\frac{3}{2} & 0 & -2 & 0 & -1 & 0 & 0 & 0 & -1 & \frac{\sqrt{3}}{2} & -\frac{3}{2} & \frac{\sqrt{3}}{2} & -\frac{1}{2} & 0 & 0 & 0 \end{bmatrix}^{\mathrm{T}} \tag{B.2}$$

KH:

$$\text{null}(\boldsymbol{A}) = \begin{bmatrix} 1 & 0 & 0 & 1 & 0 & 0 & 0 & 0 & 1 & 0 & 0 & 0 & 1 & 0 & 0 & 0 & 0 & 0 \\ 0 & 1 & 0 & 0 & 0 & 0 & 0 & 1 & 0 & 0 & 0 & 1 & 0 & 0 & 0 & 1 & 0 & 0 \\ 0 & 0 & 0 & 0 & 1 & 1 & 1 & 0 & 0 & 0 & 0 & 0 & 0 & 0 & 0 & 0 & 1 & 0 \end{bmatrix}^{\mathrm{T}} \tag{B.3}$$

$$\text{null}(\boldsymbol{B}_{\text{aug}}) = \begin{bmatrix} \frac{1}{2} & -\frac{\sqrt{3}}{6} & 0 & 0 & 1 & 0 & \frac{1}{2} & -\frac{\sqrt{3}}{6} & \frac{1}{2} & -\frac{\sqrt{3}}{2} & \frac{1}{2} & -\frac{\sqrt{3}}{6} & \frac{1}{2} & -\frac{\sqrt{3}}{2} & 1 & 0 & 0 & 0 & 0 & 0 & 0 \\ 1 & 0 & 1 & 0 & 1 & 0 & 1 & 0 & 1 & 0 & 1 & 0 & 1 & 0 & 1 & 0 & 1 & 0 & 0 & 0 & 0 \\ 0 & 1 & 0 & 1 & 0 & 1 & 0 & 1 & 0 & 1 & 0 & 1 & 0 & 1 & 0 & 1 & 0 & 1 & 0 & 0 & 0 \end{bmatrix}^{\mathrm{T}} \tag{B.4}$$

DK:

$$\text{null}(\boldsymbol{A}) = \begin{bmatrix} 1 & 0 & 0 & 0 & 0 & 0 & 0 & 0 & 0 & 1 & 0 & 0 & 0 & 0 & 0 & 1 & 0 & 1 & 0 & 0 & 0 & 0 & 0 & 0 \\ 0 & 0 & 1 & 1 & 0 & 0 & 0 & 0 & 0 & 0 & 1 & 0 & 0 & 0 & 0 & 0 & 0 & 0 & 0 & 1 & 0 & 0 & 0 & 0 \\ 0 & 0 & 0 & 0 & 0 & 0 & 0 & 0 & 1 & 0 & 0 & 0 & 0 & 0 & 1 & 0 & 0 & 0 & 1 & 0 & 1 & 0 & 0 & 0 \\ 0 & 0 & 0 & 0 & 0 & 1 & 1 & 1 & 0 & 0 & 0 & 0 & 0 & 0 & 0 & 0 & 0 & 0 & 0 & 0 & 0 & 1 & 0 & 0 \\ 0 & 1 & 0 & 0 & 1 & 0 & 0 & 0 & 0 & 0 & 0 & 0 & 0 & 0 & 0 & 0 & 1 & 0 & 0 & 0 & 0 & 0 & 1 & 0 \\ 0 & 0 & 0 & 0 & 0 & 0 & 0 & 0 & 0 & 0 & 0 & 1 & 1 & 1 & 0 & 0 & 0 & 0 & 0 & 0 & 0 & 0 & 0 & 1 \end{bmatrix}^{\mathrm{T}} \tag{B.5}$$

$$\text{null}(\boldsymbol{B}_{\text{aug}}) = \begin{bmatrix} 0 & 0 & 0 & 0 & 0 & 0 & \frac{\sqrt{3}}{2} & \frac{1}{2} & \frac{\sqrt{3}}{2} & -\frac{1}{2} & \frac{\sqrt{3}}{2} & -\frac{1}{2} & \frac{\sqrt{3}}{2} & \frac{1}{2} & 0 & 0 & 0 & 0 & 0 & 0 & 0 & 0 & 0 & 0 & 0 & 0 & 0 \\ -\frac{\sqrt{3}}{2} & \frac{1}{2} & 0 & 0 & -\frac{\sqrt{3}}{2} & \frac{1}{2} & 0 & 0 & 0 & 0 & 0 & 0 & 0 & 1 & 0 & 1 & 0 & 0 & 0 & 0 & 0 & 0 & 0 & 0 & 0 & 0 & 0 \\ \frac{\sqrt{3}}{2} & \frac{1}{2} & 0 & 0 & 0 & 0 & 0 & 0 & 0 & 1 & 0 & 0 & 0 & 0 & 0 & 0 & 0 & 0 & 0 & 1 & 0 & 0 & \frac{\sqrt{3}}{2} & \frac{1}{2} & 0 & 0 & 0 \\ 0 & 0 & \frac{\sqrt{3}}{2} & \frac{1}{2} & \frac{\sqrt{3}}{2} & \frac{1}{2} & 0 & 0 & 0 & 0 & 0 & 1 & 0 & 0 & 0 & 0 & 0 & 0 & 0 & 0 & 1 & 0 & 0 & 0 & 0 & 0 & 0 \\ 0 & 1 & 0 & 1 & 0 & 1 & 0 & 1 & 0 & 1 & 0 & 1 & 0 & 1 & 0 & 1 & 0 & 1 & 0 & 1 & 0 & 1 & 0 & 1 & 0 & 0 & 0 \\ 1 & 0 & 1 & 0 & 1 & 0 & 1 & 0 & 1 & 0 & 1 & 0 & 1 & 0 & 1 & 0 & 1 & 0 & 1 & 0 & 1 & 0 & 1 & 0 & 0 & 0 & 0 \end{bmatrix}^{\mathrm{T}} \tag{B.6}$$

MD:

$$\text{null}(\boldsymbol{A}) = \begin{bmatrix} 0 & -\frac{\sqrt{3}}{2} & 0 & 0 \\ -1 & -\frac{1}{2} & 0 & 0 \\ 1 & 0 & 0 & -\frac{1}{2} \\ 0 & 1 & 0 & -\frac{1}{2} \\ -\frac{\sqrt{3}}{2} & 0 & 0 & 0 \\ -\frac{1}{2} & -1 & 0 & 0 \\ 0 & -\frac{1}{2} & -1 & 0 \\ -\frac{1}{2} & 0 & -1 & 0 \\ -1 & -1 & 0 & -\frac{1}{2} \\ 0 & -\frac{\sqrt{3}}{2} & 0 & -\frac{\sqrt{3}}{2} \\ -\frac{\sqrt{3}}{2} & 0 & 0 & -\frac{\sqrt{3}}{2} \\ 0 & 0 & 1 & -\frac{1}{2} \\ 0 & 1 & 0 & -\frac{1}{2} \\ 0 & -1 & -1 & -\frac{1}{2} \\ 0 & 0 & 1 & -\frac{1}{2} \\ -1 & 0 & -1 & -\frac{1}{2} \\ 1 & 0 & 0 & -\frac{1}{2} \\ 0 & -1 & -\frac{1}{2} & 0 \\ 0 & 0 & -\frac{\sqrt{3}}{2} & -\frac{\sqrt{3}}{2} \\ -1 & 0 & -\frac{1}{2} & 0 \\ 0 & 0 & -\frac{\sqrt{3}}{2} & -\frac{\sqrt{3}}{2} \\ -1 & 0 & -1 & -\frac{1}{2} \\ 0 & -1 & -1 & -\frac{1}{2} \\ -\frac{\sqrt{3}}{2} & 0 & 0 & -\frac{\sqrt{3}}{2} \\ 0 & -\frac{\sqrt{3}}{2} & 0 & -\frac{\sqrt{3}}{2} \\ -1 & -1 & 0 & -\frac{1}{2} \\ -\frac{1}{2} & -1 & 0 & 0 \\ 0 & 1 & 0 & -\frac{1}{2} \\ 1 & 0 & 0 & -\frac{1}{2} \\ -1 & -\frac{1}{2} & 0 & 0 \\ 0 & -\frac{\sqrt{3}}{2} & 0 & 0 \\ 0 & 0 & -\frac{\sqrt{3}}{2} & 0 \\ -1 & 0 & -\frac{1}{2} & 0 \\ 1 & 0 & 0 & -\frac{1}{2} \\ 0 & 0 & 1 & -\frac{1}{2} \\ -\frac{1}{2} & 0 & -1 & 0 \\ -\frac{\sqrt{3}}{2} & 0 & 0 & 0 \\ 0 & 0 & -\frac{\sqrt{3}}{2} & 0 \\ 0 & -1 & -\frac{1}{2} & 0 \\ 0 & 1 & 0 & -\frac{1}{2} \\ 0 & 0 & 1 & -\frac{1}{2} \\ 0 & -\frac{1}{2} & -1 & 0 \end{bmatrix}, \quad \text{null}(\boldsymbol{B}_{\text{aug}}) = \begin{bmatrix} 0 & 0 & 1 & 0 \\ 0 & 1 & 0 & -1 \\ 0 & 0 & 1 & 0 \\ 0 & 1 & 0 & 0 \\ 0 & 0 & 1 & 0 \\ 0 & 1 & 0 & 1 \\ -\frac{\sqrt{3}}{3} & 0 & 1 & -\frac{2\sqrt{3}}{3} \\ 1 & 1 & 0 & 1 \\ \frac{\sqrt{3}}{3} & 0 & 1 & -\frac{\sqrt{3}}{3} \\ 1 & 1 & 0 & 0 \\ 0 & 0 & 1 & \frac{\sqrt{3}}{2} \\ 0 & 1 & 0 & -\frac{1}{2} \\ 0 & 0 & 1 & \frac{\sqrt{3}}{2} \\ 0 & 1 & 0 & \frac{1}{2} \\ -\frac{\sqrt{3}}{3} & 0 & 1 & -\frac{\sqrt{3}}{6} \\ 1 & 1 & 0 & \frac{1}{2} \\ -\frac{\sqrt{3}}{3} & 0 & 1 & -\frac{\sqrt{3}}{6} \\ 1 & 1 & 0 & \frac{3}{2} \\ \frac{\sqrt{3}}{3} & 0 & 1 & \frac{\sqrt{3}}{6} \\ 1 & 1 & 0 & -\frac{1}{2} \\ \frac{\sqrt{3}}{3} & 0 & 1 & \frac{\sqrt{3}}{6} \\ 1 & 1 & 0 & \frac{1}{2} \\ -\frac{\sqrt{3}}{3} & 0 & 1 & \frac{\sqrt{3}}{3} \\ 1 & 1 & 0 & 0 \\ -\frac{\sqrt{3}}{3} & 0 & 1 & \frac{\sqrt{3}}{3} \\ 1 & 1 & 0 & 1 \\ \frac{\sqrt{3}}{3} & 0 & 1 & \frac{2\sqrt{3}}{3} \\ 1 & 1 & 0 & 0 \\ \frac{\sqrt{3}}{3} & 0 & 1 & \frac{2\sqrt{3}}{3} \\ 1 & 1 & 0 & 1 \\ \frac{\sqrt{3}}{3} & 0 & 1 & -\frac{\sqrt{3}}{3} \\ 1 & 1 & 0 & 1 \\ -\frac{\sqrt{3}}{3} & 0 & 1 & -\frac{2\sqrt{3}}{3} \\ 1 & 1 & 0 & 0 \\ \frac{\sqrt{3}}{3} & 0 & 1 & \frac{\sqrt{3}}{6} \\ 1 & 1 & 0 & \frac{3}{2} \\ -\frac{\sqrt{3}}{3} & 0 & 1 & -\frac{\sqrt{3}}{6} \\ 1 & 1 & 0 & -\frac{1}{2} \\ 0 & 0 & 1 & -\frac{\sqrt{3}}{2} \\ 0 & 1 & 0 & -\frac{1}{2} \\ 0 & 0 & 1 & -\frac{\sqrt{3}}{2} \\ 0 & 1 & 0 & \frac{1}{2} \\ 0 & 0 & 0 & 0 \\ 0 & 0 & 0 & 0 \\ 0 & 0 & 0 & 0 \end{bmatrix} \tag{B.7}$$

C

Periodic boundary conditions for symmetric rectangular 2D unit cells

Periodic boundary conditions are a powerful means to represent infinitely large repetitive structures. One-fourth of a lattice material unit cell can be sufficient to determine the effective macroscopic elastic properties. Generally, such a cell contains only a limited number of struts and thus can be modelled at very low computational cost. The approach is most effective when the unit cell and load share lines of symmetry. Effective macroscopic properties can be determined from uniaxial stress/strain load cases, which have clear symmetry properties. Any 2D repetitive structure can be represented by an unlimited number of different unit cells, therefore one that features the appropriate symmetries can often be selected.

Fig. C.1a schematically shows a unit cell with two lines of symmetry: horizontal symmetry w.r.t. $x_1 = 0$ and vertical symmetry w.r.t. $x_2 = 0$. It is chosen to model the top-right quarter here, shown in figure C.1b. It depicts the unit cell sustaining a uniaxial stress state: $\sigma_{11} \neq 0$, $\sigma_{22} = \sigma_{12} = 0$. Note that this load shares both axes of symmetry with the unit cell. For any structure, it is well known that nodes that lie on an axis of symmetry do not displace orthogonal to that line of symmetry under a symmetric load. In this case:

$$u_1|_{x_1=0} = 0, \quad u_2|_{x_2=0} = 0. \tag{C.1}$$

Also, a symmetric response requires the rotations along an axis of symmetry to be zero:

$$\varphi|_{x_1=0} = 0, \quad \varphi|_{x_2=0} = 0. \tag{C.2}$$

Displacements and rotations at equal distances from either side of an axis of symmetry are related:

$$u_1|_{x_1=a} = -u_1|_{x_1=-a}\,, \qquad u_2|_{x_1=a} = u_2|_{x_1=-a}\,, \tag{C.3a}$$

$$u_1|_{x_2=b} = u_1|_{x_2=-b}\,, \qquad u_2|_{x_2=b} = -u_2|_{x_2=-b}\,, \tag{C.3b}$$

$$\varphi|_{x_1=\frac{1}{2}W} = -\varphi|_{x_1=-\frac{1}{2}W}\,, \tag{C.3c}$$

$$\varphi|_{x_2=\frac{1}{2}H} = -\varphi|_{x_2=-\frac{1}{2}H}. \tag{C.3d}$$

On the other hand, the unit cell must 'fit' the cell to the left, right, top and bottom of it, even after deformation. That is, periodicity requires the unit cell to keep its rectangular shape , and enforces the rotations of 'connected' nodes on the left and right c.q. top and bottom boundaries to be equal:

$$u_1|_{x_1=\frac{1}{2}W} = \frac{1}{2}W\varepsilon_{11}, \tag{C.4a}$$

$$u_2|_{x_2=\frac{1}{2}H} = \frac{1}{2}H\varepsilon_{22}, \tag{C.4b}$$

$$\varphi|_{x_1=\frac{1}{2}W} = \varphi|_{x_1=-\frac{1}{2}W}, \tag{C.4c}$$

$$\varphi|_{x_2=\frac{1}{2}H} = \varphi|_{x_2=-\frac{1}{2}H}. \tag{C.4d}$$

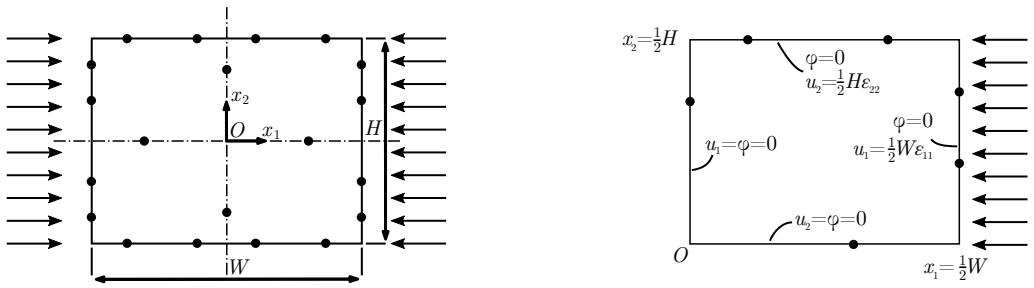

(a) (b)

Figure C.1: (a) Rectangular unit cell with two lines of symmetry under uniaxial stress. (b) Right-top quarter of the unit cell, symmetry and periodic boundary conditions indicated.

Note that the pairs of equations C.3c & C.4c and C.3d & C.4d can only be simultaneously satisfied if

$$\varphi|_{x_1=\frac{1}{2}W} = \varphi|_{x_1=-\frac{1}{2}W} = 0 \text{ and} \tag{C.5a}$$

$$\varphi|_{x_2=\frac{1}{2}H} = \varphi|_{x_2=-\frac{1}{2}H} = 0 \tag{C.5b}$$

Figure C.1b shows all boundary conditions required to model uniaxial compression of a symmetric 2D repetitive structure. Of course, only one of ε_{11} and ε_{22} is prescribed. The other measure of effective strain follows from the model. It is necessary to equate all the outward displacements of the nodes on the 'free' boundary to each other: this ensures that the cell stays rectangular.

D

Stiffness of KT and KH lattices

Figs. D.1 and D.2 show side-by-side comparisons of KT and KH geometries under 11-compression. Note that the results are for $\bar{\rho} = 0.3$, at which beam theory yields no accurate representation of reality as slenderness ratios of the members are far below 1:10. Still, these figures clarify how the loads are distributed in the members of the two structures, and constitute their macroscopic stiffness.

Fig. D.1 shows the axial forces that occur in the members. Transverse forces are illustrated in Fig. D.2. The absolute values of these forces are insignificant as the results are normalised. The ratios are of importance; the axial forces in the KH unit cell are lower than in the KT unit cell. If only axial stiffness, i.e. the stretching of members were considered, the KT structure would be stiffer than the KH structure. Looking at the transverse forces which arise due to bending on the other hand; these are higher in the deformed KH unit cell. Therewith the KH structure 'compensates' its total macroscopic stiffness, especially with decreasing slenderness (and thus increasing density). This explains both why the Young's moduli for these structures are very similar, and why the elastic moduli and Poisson's ratio of KH vary visibly non-linearly with increasing relative density.

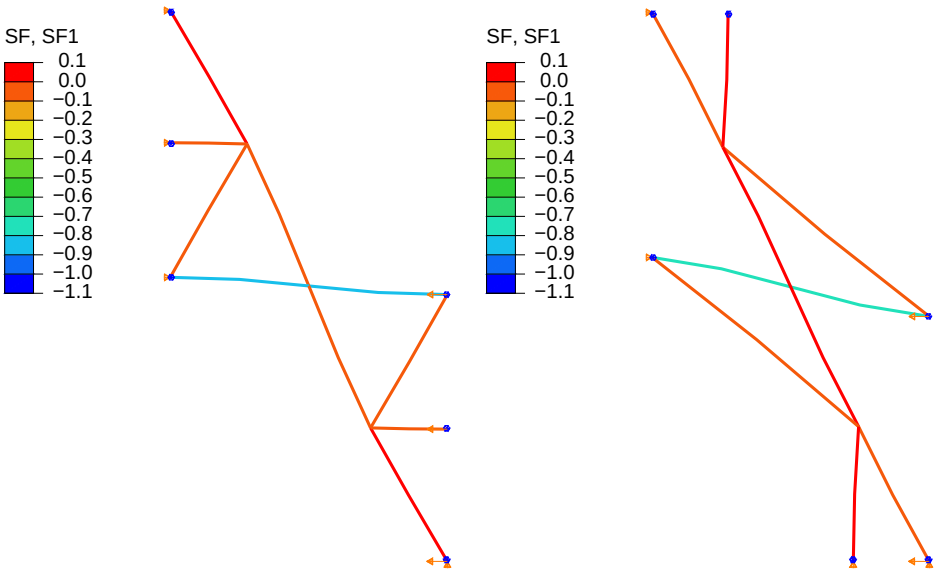

(a) (b)

Figure D.1: Axial force levels in a (a) KT and (b) KH unit cell under 11-compression. $\bar{\rho} = 0.3$. Displayed displacements are greatly magnified.

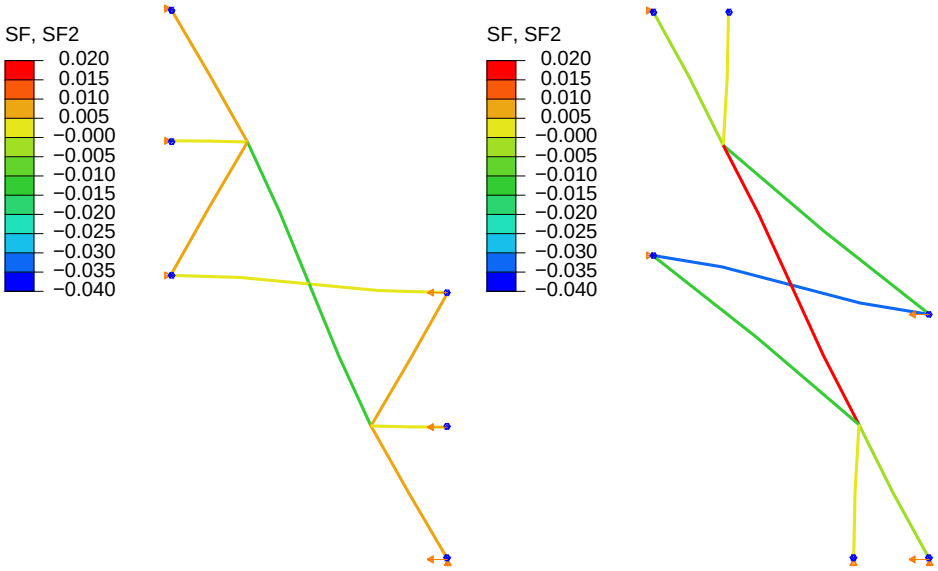

(a) (b)

Figure D.2: Transverse force levels in a (a) KT and (b) KH unit cell under 11-compression. $\bar{\rho} = 0.3$. Displayed displacements are greatly magnified.

E

Matrix analysis of the triangulated structure

Matrix analysis was performed for the triangulated micro-architecture for comparison with the novel structures through table 7.1. The unit cell used is shown in Fig. E.1. One-fourth of this unit cell, containing only one node, is also a translational unit cell. That smaller unit cell is not suited for matrix analysis as through periodicity, both ends of its members are connected to the same node. That results in equilibrium and compatibility matrices filled with zeroes.

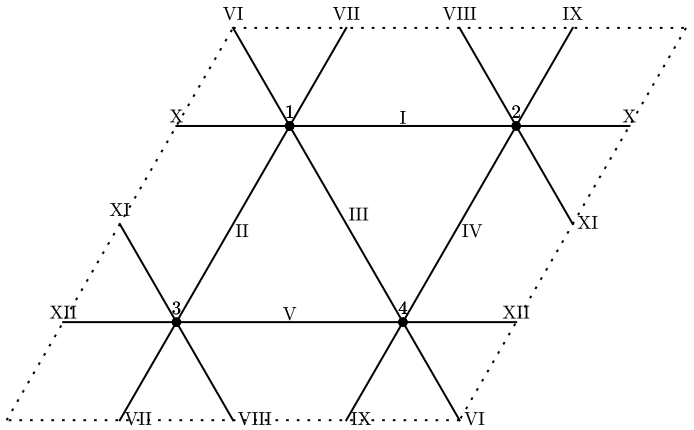

Figure E.1: Unit cell for matrix analysis of the Triangular structure.

With its nodal connectivity of 6, this structure does not satisfy Eq. (2.4) and thus does not have square equilibrium and compatibility matrices. The 8×12 equilibrium matrix reads:

$$\boldsymbol{A} = \begin{bmatrix} -1 & \frac{1}{2} & -\frac{1}{2} & 0 & 0 & \frac{1}{2} & -\frac{1}{2} & 0 & 0 & 1 & 0 & 0 \\ 0 & \frac{\sqrt{3}}{2} & \frac{\sqrt{3}}{2} & 0 & 0 & -\frac{\sqrt{3}}{2} & -\frac{\sqrt{3}}{2} & 0 & 0 & 0 & 0 & 0 \\ 1 & 0 & 0 & \frac{1}{2} & 0 & 0 & 0 & \frac{1}{2} & -\frac{1}{2} & -1 & -\frac{1}{2} & 0 \\ 0 & 0 & 0 & \frac{\sqrt{3}}{2} & 0 & 0 & 0 & -\frac{\sqrt{3}}{2} & -\frac{\sqrt{3}}{2} & 0 & \frac{\sqrt{3}}{2} & 0 \\ 0 & -\frac{1}{2} & 0 & 0 & -1 & 0 & \frac{1}{2} & -\frac{1}{2} & 0 & 0 & \frac{1}{2} & 1 \\ 0 & -\frac{\sqrt{3}}{2} & 0 & 0 & 0 & 0 & \frac{\sqrt{3}}{2} & \frac{\sqrt{3}}{2} & 0 & 0 & -\frac{\sqrt{3}}{2} & 0 \\ 0 & 0 & \frac{1}{2} & -\frac{1}{2} & 1 & -\frac{1}{2} & 0 & 0 & \frac{1}{2} & 0 & 0 & -1 \\ 0 & 0 & -\frac{\sqrt{3}}{2} & -\frac{\sqrt{3}}{2} & 0 & \frac{\sqrt{3}}{2} & 0 & 0 & \frac{\sqrt{3}}{2} & 0 & 0 & 0 \end{bmatrix}, \tag{E.1}$$

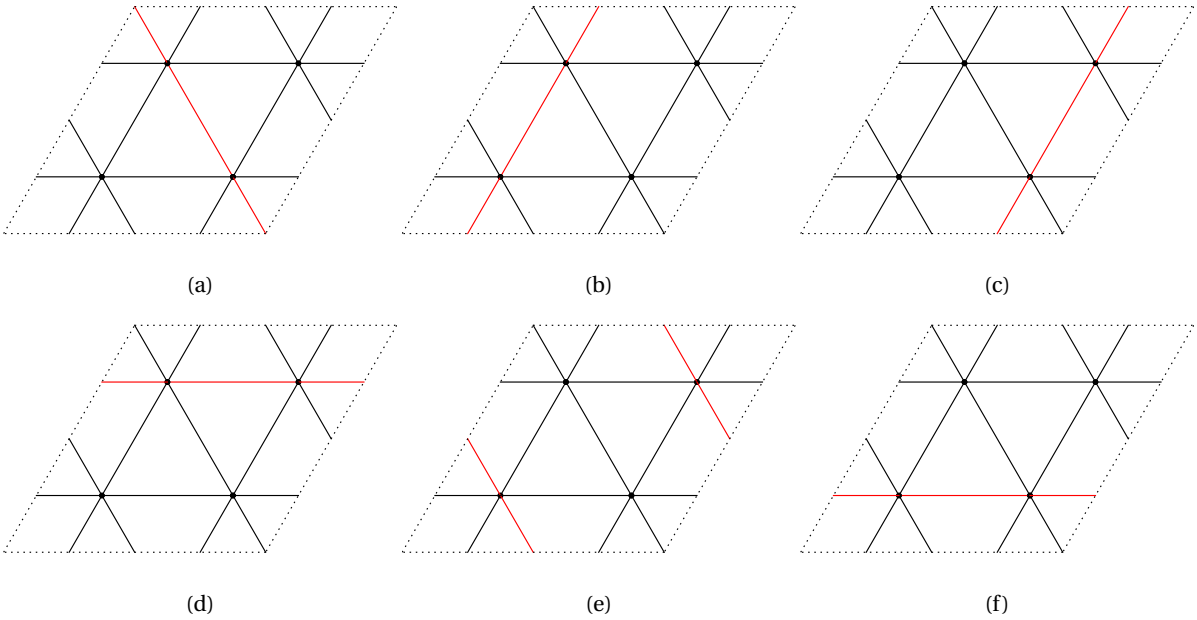

Figure E.2: The six linearly independent states of self stress of the Triangular structure. Red members sustain (unity) tension, black struts are tension-free.

which is of rank 6 and thus rank-deficient by $s = 6$. Its nullspace reads:

$$\text{null}(\boldsymbol{A}) = \begin{bmatrix} 0 & 0 & 1 & 0 & 0 & 1 & 0 & 0 & 0 & 0 & 0 & 0 \\ 0 & 1 & 0 & 0 & 0 & 0 & 1 & 0 & 0 & 0 & 0 & 0 \\ 0 & 0 & 0 & 1 & 0 & 0 & 0 & 0 & 1 & 0 & 0 & 0 \\ 1 & 0 & 0 & 0 & 0 & 0 & 0 & 0 & 0 & 1 & 0 & 0 \\ 0 & 0 & 0 & 0 & 0 & 0 & 0 & 1 & 0 & 0 & 1 & 0 \\ 0 & 0 & 0 & 0 & 1 & 0 & 0 & 0 & 0 & 0 & 0 & 1 \end{bmatrix}^{\mathrm{T}}, \tag{E.2}$$

each of the vectors in which represents a set of aligned members in the structure sustaining the same tension, see figure E.2. Note that these states of self-stress are equivalent in pairs of two. Also, they are very similar to the stress-states found for the KT, KH and DK structures in Chapter 4; using the method of sections it is easily verified that $S = 3$ for a triangular periodic truss.

The 12×8 compatibility matrix $\boldsymbol{B} = \boldsymbol{A}^{\mathrm{T}}$ is also of rank 6 and therefore rank-deficient by $m = 2$. Its nullspace reads:

$$\text{null}(\boldsymbol{B}) = \begin{bmatrix} 1 & 0 & 1 & 0 & 1 & 0 & 1 & 0 \\ 0 & 1 & 0 & 1 & 0 & 1 & 0 & 1 \end{bmatrix}^{\mathrm{T}}, \tag{E.3}$$

and only contains the two 2D rigid-body translations.

Bibliography

[1] M. F. Ashby, A. G. Evans, N. A. Fleck, L. J. Gibson, J. W. Hutchinson, and H. N. G. Wadley. *Metal Foams: A Design Guide*. Butterworth-Heinemann, Oxford, 2000.

[2] H. Aslaksen. In search of demiregular tilings. In Reza Sarhangi and John Sharp, editors, *BRIDGES Mathematical Connections in Art, Music, and Science*, pages 533–536. tarquin publications, 2006.

[3] C. Ayas and C. Tekoglu. On the sufficient symmetry conditions for isotropy of elastic moduli. *Journal of Applied Mechanics*, Submitted for publication.

[4] K. Critchlow. *Order in Space: A Design Source Book*. Viking Press, 1970.

[5] V. S. Deshpande, M. F. Ashby, and N. A. Fleck. Foam topology: Bending versus stretching dominated architectures. *Acta Materialia*, 49(6):1035–1040, 2001.

[6] A. Donev and S. Torquato. Energy-efficient actuation in infinite lattice structures. *Journal of the Mechanics and Physics of Solids*, 51(8):1459 – 1475, 2003.

[7] S. L. dos Santos e Lucato, J. Wang, P. Maxwell, R. M. McMeeking, and A. G. Evans. Design and demonstration of a high authority shape morphing structure. *International Journal of Solids and Structures*, 41 (13):3521 – 3543, 2004.

[8] S. L. dos Santos e Lucato, R. M. McMeeking, and A. G. Evans. Actuator placement optimization in a kagome based high authority shape morphing structure. *Smart Materials and Structures*, 14(4):869–875, 2005.

[9] N. A. Fleck. An overview of the mechanical properties of foams and periodic lattice materials. In V. Altstadt R.F. Singer, C. Korner and H. Munstedt, editors, *Cellular Metals and Polymers*, volume 44. Trans Tech Publications, 2004.

[10] L. J. Gibson and M. F. Ashby. *Cellular Solids: Structure and Properties*. Cambridge University Press, Cambridge, 2 edition, 1997.

[11] S. D. Guest and J. W. Hutchinson. On the determinacy of repetitive structures. *Journal of the Mechanics and Physics of Solids*, 51(3):383–391, 2003.

[12] Z. Hashin and S. Shtrikman. A variational approach to the theory of the elastic behaviour of multiphase materials. *Journal of the Mechanics and Physics of Solids*, 11:127–140, 1963.

[13] R. G. Hutchinson and N. A. Fleck. The structural performance of the periodic truss. *Journal of the Mechanics and Physics of Solids*, 54(4):756 – 782, 2006.

[14] R. G. Hutchinson, N. Wicks, A. G. Evans, N. A. Fleck, and J. W. Hutchinson. Kagome plate structures for actuation. *International Journal of Solids and Structures*, 40(25):6969 – 6980, 2003.

[15] S. Hyun and S. Torquato. Optimal and manufacturable two-dimensional, kagome-like cellular solids. *Journal of Materials Research*, 17:137–144, 1 2002. ISSN 2044-5326.

[16] Fraunhofer IFAM. Open-cell metal foams. https://www.ifam.fraunhofer.de/en/Profile/Locations/Dresden/Cellular_metallic_
2018. Accessed 17-2-2018.

[17] A.C.H Leung and S.D. Guest. Actuation-softening in kagome lattice structures. In *47th AIAA/ASME/ASCE/AHS/ASC Structures, Structural Dynamics, and Materials Conference*. American Institute of Aeronautics and Astronautics, 2006.

[18] S. Li. Boundary conditions for unit cells from periodic microstructures and their implications. *Composites Science and Technology*, 68:1962–1974, 2008.

[19] S.P Mai and N.A Fleck. Reticulated tubes: effective elastic properties and actuation response. *Proceedings of the Royal Society of London A: Mathematical, Physical and Engineering Sciences*, 465(2103): 685–708, 2009. ISSN 1364-5021.

[20] J. C. Maxwell. On the calculation of the equilibrium and stiffness of frames. *Philosophical Magazine*, 27 (182):294–299, 1864. (Paper XXVI in Collected Papers, Cambridge University Press, 1890).

[21] P. R. Onck. Cosserat modeling of cellular solids. *Comptes Rendus Mécanique*, 330(11):717 – 722, 2002. ISSN 1631-0721.

[22] S. Pellegrino and C. R. Calladine. Matrix analysis of statically and kinematically indeterminate frameworks. *International Journal of Solids and Structures*, 22(4):409 – 428, 1986.

[23] T. N. Pronk. A quest for lattice materials for actuation. Master's thesis, Delft University of Technology, June 2016.

[24] T.N. Pronk, C. Ayas, and C. Tekoğlu. A quest for 2d lattice materials for actuation. *Journal of the Mechanics and Physics of Solids*, 105:199–216, 2017.

[25] T.A. Schaedler, A.J. Jacobsen, A. Torrents, A.E. Sorensen, J.Lian, J.R. Greer, L. Valdevit, and W.B. Carter. Ultralight metallic microlattices. *Science*, 334:962–965, 2011.

[26] A. Vigliotti and D. Pasini. Analysis and design of lattice materials for large cord and curvature variations in skin panels of morphing wings. *Smart Materials and Structures*, 24(3):037006, 2015.

[27] A.-J. Wang and D.L. McDowell. In-plane stiffness and yield strength of periodic metal honeycombs. *Journal of Engineering Materials and Technology*, 126:137 – 156, April 2004.

[28] N. Wicks and S. D. Guest. Single member actuation in large repetitive truss structures. *International Journal of Solids and Structures*, 41(3-4):965 – 978, 2004.

[29] N. Wicks and J. W. Hutchinson. Sandwich plates actuated by a kagome planar truss. *Journal of Applied Mechanics*, 71(5):652–662, 2004.

[30] X. Zheng, H. Lee, T H. Weisgraber, and M. Shusteff. Ultralight, ultrastiff mechanical metamaterials. *Science*, 344:1373–1377, June 2014.